DEVELOPMENT OF AN UNSTEADY ATMOSPHERIC BOUNDARY LAYER MODEL

UTVECKLING AV EN ICKE-STATIONÄR GRÄNSSKIKTSMODELL

by Svante Bodin

SMHI Rapporter

METEOROLOGI OCH KLIMATOLOGI

Nr RMK 2 (1974)

SVERIGES METEOROLOGISKA OCH HYDROLOGISKA INSTITUT

DEVELOPMENT OF AN UNSTEADY ATMOSPHERIC BOUNDARY LAYER MODEL

UTVECKLING AV EN ICKE-STATIONÄR GRÄNSSKIKTSMODELL

by Svante Bodin

SMHI Rapporter

METEOROLOGI OCH KLIMATOLOGI

Nr RMK 2 (1974)

SVERIGES METEOROLOGISKA OCH HYDROLOGISKA INSTITUT

Stockholm 1974

Corrections

Page 5, bottom line:

..... quantities but as mean quantities (deviations), which are the

Page 10, line 4:

.... Fig. 1 shows

Page 10, line 24:

the same variation of $\mathbb{V}^*$ as used for $\mathbb{V}_g$ in the Ching & Businger

Page 10, bottom line:

mass field by means of inertial oscillations.

Page 11, line 20:

in the pressure gradient, which are enhanced when $\alpha \sim f$.

Page 12, line 16, 17, 19 and 20:

l should read ℓ

Page 14, eq. (19):

$$Z = a \cdot \frac{k^y - 1}{k - 1} \qquad \text{or} \qquad y = \frac{1}{\log k} \cdot \log\left(\frac{k-1}{a} \cdot Z + 1\right)$$

Page 17, line 14:

$$(26) \qquad T(z,t) = T_D + \frac{T_0 - T_D}{D}(D - z) + \frac{2}{D} \sum_{n=1}^{\infty} e^{-\frac{n^2\pi^2 K_s t}{D^2}} \sin\frac{n\pi}{D} z \int_0^D h(z') \sin\frac{n\pi}{D} \cdot Z' dz' - \frac{2}{\pi} \sum_{n=1}^{\infty} \frac{1}{n} e^{-\frac{n^2\pi^2 K_s t}{D^2}} \sin\frac{n\pi}{D} z \int_0^t \frac{\partial T_0}{\partial t'} e^{\frac{n^2\pi^2 K_s t'}{D^2}} dt'$$

Page 20, line 17:

..... It shows that (29.1) does not give

Page 25, second line from the bottom:

.... boundary layer models during a visit to

TABLE OF CONTENTS

	Summaries (English, Swedish)	page 1
1	Introduction	" 3
2	Derivation of model equations	" 5
3	Filtering of inertial-diffusive oscillations ...	" 9
4	Formulation of K for neutral and stable stratification	" 11
5	Numerical solution	" 13
6	Heat conduction in the soil and heat flux at the earth's surface	" 16
7	Results of numerical integrations	" 20
8	Conclusions and discussion	" 24
	Figures 1-15	" 26-40
	References	" 41

SUMMARY

To serve as an aid in preparing local forecasts as well as landing forecasts at airports, a development of an atmospheric boundary layer model has been started at SMHI. The model is going to use large scale wind, temperature and moisture predictions from a numerical weather prediction model as variable boundary conditions. Instead of using the ordinary Ekman boundary layer equations an approach due to L N Gutman (1969) has been used in deriving a set of one-dimensional boundary layer equations. It is shown that this formulation filters out inertial- diffusive oscillations, which are present in an Ekman boundary layer due to time variations in the geostrophic wind.

Experiments with variable large scale winds have been done, using a simple dry model with prescribed variations in the boundary values for wind and temperature. A turbulent exchange coefficient formulation has been used, which is based on Monin & Obukhov´s similarity theory and which uses a mixing length formulation due to Blackadar. For the numerical solution a Crank-Nicolson scheme has been used. The computations show large differences between the steady state and the unsteady state solutions. This is shown in wind hodographs as well as in time functions of friction velocity, u_*, and cross isobar angle. Finally, from two different analytical solutions as well as a finite difference solution of the heat conduction equation, heat fluxes at the earth´s surface due to heat conduction in the soil have been computed. These analytical solutions have been compared in terms of accuracy and efficiency.

SAMMANDRAG

För att tjäna som ett hjälpmedel för lokalprognoser och flygplatsprognoser har vid SMHI startats ett arbete med att utveckla en atmosfärisk gränsskiktsmodell. Modellen ska kopplas till en storskalig, numerisk prognosmodell som förser den med variabla randvärden för vind, temperatur och fuktighet. Istället för att använda de vanliga Ekman-ekvationerna har använts en metod utvecklad av L N Gutman (1969) för att härleda gränsskiktsekvationer för en en-dimensionell modell. Dessa ekvationer har fördelen att de filtrerar bort de tröghet-diffusionssvängningar som är närvarande i ett Ekman-skikt när den geostrofiska vinden varierar i tiden.

En enkel, torr version av modellen har utnyttjats för att studera effekten av variationen i tiden av bakgrundsvinden (den storskaliga vinden). En turbulent utbyteskoefficient, som är grundad på Monin & Obukhovs similaritetsteori och som använder Blackadars reduktion av blandningslängden, har använts i dessa experiment. Crank-Nicolson-metoden har utnyttjats vid den numeriska tidsintegrationen. Beräkningsresultaten visar att det blir stora skillnader mellan vinden beräknad ur den icke-stationära modellen och motsvarande stationära lösningar. Detta visas med vindhodografer vid olika tidpunkter samt med figurer med friktionshastigheten, u_*, och tvärisobara vinkeln som funktion av tiden. Slutligen har också en jämförelse gjorts mellan två olika analytiska lösningar samt en finit differenslösning, från vilka värmeflödena vid jordytan, beroende på värmeledning, i marken som funktion av tiden har beräknats.

1 Introduction

1.1 At the present time numerical weather prediction models for large scale atmospheric motion are in use all over the world. They have rapidly become an integrated part in most weather services. The models can predict and describe the large scale synoptic developments fairly well but the actual interpretation of the numericl forecasts into terms of local weather is by and large left to the human forecaster. Attempts have been made along climatological/statistical lines to develop automatic interpretation programs with varying degrees of succes.

Local weather is to a large extent the result of boundary layer processes, influenced by topography, which are forced by the large scale flow. It is therefore natural to try to formulate models of the atmospheric boundary layer in order to get forecasts of temperature, wind, moisture and water content near the ground. This is particularely important as an aid in preparing landing forecasts at airports especially regarding fog conditions. The main obstacle has been a lack of an adequate parameterization of the turbulent exchange in the boundary layer, but since the development of the Monin & Obukhov similarity theory several attempts have been made to formulate and develop numerical models of the boundary layer (Estoque, 1963, Pandolfo et.al., 1965, Sasamori, 1970). Neither of them have been used operationally. These models have usually employed one-dimensional boundary layer equations of the Ekman type with an assumption of a stationary constant flux layer in the lowest part (Prandtl layer) of the boundary layer.

1.2 Another approach has been taken by L N Gutman, who is working at the Novosibirsk Computing Center. His approach seems to have certain advantages when the aim is to couple the boundary layer model to a synoptic large scale model. In many places nowaday a so called telescope technique is used in ordinary numerical forecast models in order to run the model on small, limited areas where it is possible to use high numerical resolution, i.e. small horizontal and vertical grid distances. In this technique variable boundary values are supplied to the limited area model from a run over a much larger area with less resolution. Gutman's approach is very suitable for such a technique to be applied to the atmospheric boundary layer. In Gutman (1968) sets of equations for

use in non-linear problems in meso-meteorology are derived. This study follows Gutman in its basic approach in order to derive a set of one-dimensional boundary layer equations.

The main idea in this approach is to let the boundary layer model only take care of the specific boundary layer processes, e.g. turbulence, long wave radiation etc. In the mathematical derivation this is achieved by defining two sets of equations of motion. The first set is a "complete" set of equations of motion capable of describing all types and scales of motion e.g. large scale motion, convection, mountain waves, sound waves etc. The second set consists of equations of motion corresponding to the primitive equations used in large scale numerical forecasting or synoptic scale numerical models. By subtracting the synoptic scale equations from the first, "complete", set of equations we get a new set of equations, simply describing the difference between the two, where also the boundary layer processes are included. These equations can then be further approximated according to the particular problem concerned. In our case convective motions are excluded as well as sound waves and non-linear effects in the boundary layer resulting in equations for an one-dimensional boundary layer model.

The main difference between equations arrived at in the way described above and the Ekman type of boundary layer equations is the elimination of inertial-diffusive oscillations present in the latter formulation. These are caused by unsteadyness in the pressure field, i.e. time variations in the geostrophic wind (Ching & Businger, 1968). In steady state conditions the two formulations behave similarly.

The aim with this work has been to apply Gutman's approach and to study the effect of unsteady conditions in the imposed, "forcing" large scale flow. Therefore the formulation of the turbulent exchange in this model is fairly crude. The model has also been run without moisture and radiation. This will be improved on in the future work, partly in cooperation with the Meteorological Service of the Royal Swedish Air Force.

1.3 An important part in all boundary layer models is the inclusion of a top soil layer in order to be able to compute the heat flux from the soil across the earths' surface. In this study is also

included an investigation of numerical methods to compute this heat flux. A fourier solution of the heat conduction equation for the top soil layer has been compared with ordinary finite difference methods as well as with a Greens function solution.

2 Derivation of model equations

We will in this section discuss the equations and the assumptions behind them. For a detailed discussion see Gutman (1968).

The main idea, as stated above, is to express the motion as composed of a large scale flow component and a boundary layer component. If we denote the total motion with overbar, large scale motion with a star and the BL-motion(boundary layer motion) with a prime we get following relations

$$(1)\qquad \begin{cases} \bar{u} = u^* + u' & u^* \sim u' \\ \bar{v} = v^* + v' & v^* \sim v' \\ \bar{w} = w^* + w' & w^* \lesssim w' \end{cases}$$

$$(2)\qquad \begin{cases} \bar{T} = T^* + T' \quad \bar{\theta} = \theta + \theta' & T' \ll T^* \text{(absolute temperature} \\ \bar{p} = p^* + p' & p' \ll p^* \\ \bar{q} = q^* + q' & q' < q^* \\ \bar{Q} = Q^*_q + Q'_q & Q^*_q \sim Q'_q \\ \bar{\rho} = \rho^* + \rho' & \rho' \ll \rho^* \\ \overline{\frac{\delta Q}{dt}} = \frac{\delta Q}{dt} + \frac{\delta Q'}{dt} & \frac{\delta Q^*}{dt} \sim \frac{\delta Q'}{dt} \\ \bar{K} = K^* + K' & K^* \sim K' \end{cases}$$

u, v, w, T, θ, p and ρ have their usual meaning. q is specific humidity, Q_q is a moisture source or sink term and $\frac{\delta Q}{dt}$ the corresponding term for heat (e.g. radiation, condensation etc). K is the turbulent exchange coefficient. It must be emphazised that the primed quantities are not to be considered as "fluctuating" turbulent quantities but as mean quantities (deviations), which are th

result of specific processes in the boundary layer. The turbulent parameterization is instead taken care of by means of a turbulent exchange coefficient or eddy viscosity formulation. (See fig below)

For temperature, density and pressure the boundary layer induced variations are much smaller than the corresponding large scale quantities. This is obviously not true for the wind where the adjustmen to the lower boundary condition $\bar{u} = \bar{v} = 0$ gives $u' \sim v' \sim u^* \sim v^*$.

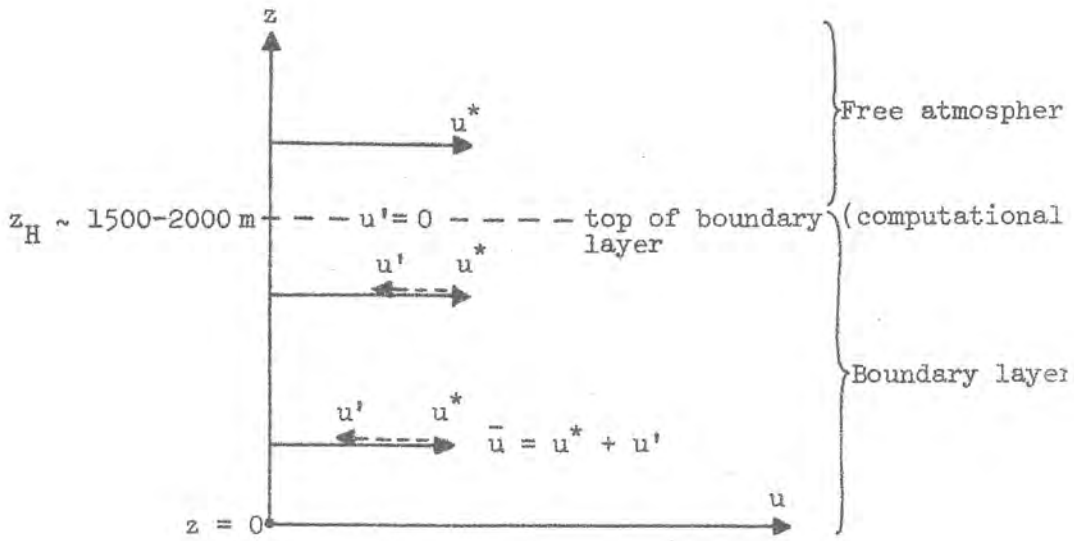

At some level we should have negligible influence from the boundary layer processes where we assume only large scale flow. Denoting this level by H we have

(3) $z = H$: $T' = p' = q' = \rho' = \theta' = Q'_q = \delta Q'/dt = u' = v' = w' = 0$

(4) $z = z_0$ zero slip conditions: $\bar{u} = \bar{v} = \bar{w} = 0$

or $u' = -u^*$, $v' = -v^*$.

T' and q' will be prescribed functions of time to start with.

The computational top of the boundary layer is taken to be high enough for the actual boundary layer height, h, to fullfill $h \leq H$

in the majority of cases, except for penetrating convection. The level H can then conveniently be taken at a height corresponding to for example the 850 mb level (~ 1 500 m).

The procedure followed to arrive at the boundary layer equations is:

a. Substitute (1) and (2) in the complete set of equations for overbar quantities.

b. Subtract the equations for the large scale flow from the resulting equations.

c. Use the << inequalities to simplify the equations (i.e. a generalized Boussinesque approximation.)

d. Assume $\frac{\partial w'}{\partial t} = 0$, that is neglect convective problems (mountain waves etc). The effect on the mean motion in the boundary layer will instead be taken care of by the turbulent terms.

e. Assume no horizontal gradients in the boundary layer variables, that is, $\nabla \mathbf{V}' = \nabla T' = \nabla q' = \nabla \rho' = 0$, horizontal homogeneity.

This implies that z_0 is constant over the influence domain. This gives us

$$
(5)\quad
\begin{cases}
(1)\quad \dfrac{\partial u'}{\partial t} = fu' + \dfrac{\partial}{\partial z}\left(K'_m \dfrac{\partial \bar{u}}{\partial z}\right) + \dfrac{\partial}{\partial z}\left(K^*_m \dfrac{\partial u'}{\partial z}\right) \\[2ex]
(2)\quad \dfrac{\partial v'}{\partial t} = -fv' + \dfrac{\partial}{\partial z}\left(K'_m \dfrac{\partial \bar{v}}{\partial z}\right) + \dfrac{\partial}{\partial z}\left(K^*_m \dfrac{\partial v'}{\partial z}\right) \\[2ex]
(3)\quad \dfrac{T^*}{\theta^*}\dfrac{\partial \theta'}{\partial t} = \dfrac{\partial}{\partial z}\left(K^*_H \dfrac{\partial \theta'}{\partial z}\right) + \dfrac{\partial}{\partial z}\left(K'_H \dfrac{\partial \bar{\theta}}{\partial z}\right) + \dfrac{1}{c_p}\dfrac{\delta Q'}{dt} \\[2ex]
(4)\quad \dfrac{\partial q'}{\partial t} = \dfrac{\partial}{\partial z}\left(K'_q \dfrac{\partial \bar{q}}{\partial z}\right) + \dfrac{\partial}{\partial z}\left(K^*_q \dfrac{\partial q'}{\partial z}\right) + Q'_q \\[2ex]
(5)\quad \rho' = 0 \ , \quad \bar{\rho} = \rho^*(z) \\[2ex]
(6)\quad \dfrac{dp^*}{dz} = -g\rho^*
\end{cases}
$$

where K_m is the eddy coefficient for momentum, K_H for the heat and K_q for moisture and water droplets. A simple scale analysis shows that if the non-linear term $\mathbf{V}'\nabla\mathbf{V}'$ is discarded then should also the term $\mathbf{V}' \cdot \nabla\mathbf{V}^*$ be neglected.

In the simplified version studied here we will further assume that the background, large scale flow, is barotropic ($\frac{\partial u^*}{\partial z} = \frac{\partial v^*}{\partial z} = 0$) and frictionless ($K^* = 0$).

This reduces the set of equations (5) to the set used in this study:

$$(6)\quad \begin{cases} \text{(a)} \quad \dfrac{\partial u'}{\partial t} = f\ v' + \dfrac{\partial}{\partial z}\left(K_m' \dfrac{\partial u'}{\partial z}\right) \\[2ex] \text{(b)} \quad \dfrac{\partial v'}{\partial t} = -\ fu' + \dfrac{\partial}{\partial z}\left(K_m' \dfrac{\partial v'}{\partial z}\right) \\[2ex] \text{(c)} \quad \dfrac{\partial \theta'}{\partial t} = \dfrac{\partial}{\partial z}\left(K_H' \dfrac{\partial \bar{\theta}}{\partial z}\right) + \dfrac{1}{c_p} \dfrac{\delta Q'}{dt} \\[2ex] \text{(d)} \quad \dfrac{\partial q'}{\partial t} = \dfrac{\partial}{\partial z}\left(K_q' \dfrac{\partial \bar{q}}{\partial z}\right) + Q_q' \end{cases}$$

where

$$(7)\quad \begin{cases} u' = \bar{u} - u^* \\ v' = \bar{v} - v^* \\ \theta' = \bar{\theta} - \theta^* \\ q' = \bar{q} - q^* \end{cases}$$

We have also assumed $T^*/\theta^* \approx 1$, which is a good approximation in the boundary layer of depth ~ 1 000 m. In the experiments carried out so far the boundary layer is assumed dry, that is eq. (6 d) is not used.

$$
\begin{cases}
(a) \quad \dfrac{\partial \rho}{\partial t} + \nabla \cdot (\rho \mathbf{v}) = 0 \\
(b) \quad \dfrac{\partial \mathbf{v}}{\partial t} = -\dfrac{1}{\rho} \nabla p + \nu \nabla^2 \mathbf{v} \\
(c) \quad \dfrac{\partial T}{\partial t} = \dfrac{1}{\rho c_p} (k \nabla^2 T) - \dfrac{p}{\rho c_p} \nabla \cdot \mathbf{v} \\
(d) \quad p = \dfrac{\rho}{m} (k_B T)
\end{cases}
\tag{6}
$$

where,

The boundary conditions for (6) are:

$$\underline{z = z_0}: \quad T' = T_0(t) \quad , \quad q' = q_0(t)$$

$$u' = - u^*(t)$$

$$v' = - v^*(t)$$

$$\underline{z = H}: \quad u' = v' = T' = q' = 0$$

The set of equations, (6), is consistent in the sense that if we put all primed quantities equal to zero it yields a set of identities, where the flow is entirely described by the large scale equations.

The main difference between (6) and a usual set of Ekman type boundary layer equations

$$(8) \quad \begin{cases} \dfrac{\partial u}{\partial t} = f\,(v - v_g) + \dfrac{\partial}{\partial z}\left(K \dfrac{\partial u}{\partial z}\right. \\ \\ \dfrac{\partial v}{\partial t} = f\,(u - u_g) + \dfrac{\partial}{\partial z}\left(K \dfrac{\partial v}{\partial z}\right) \end{cases}$$

are

1. inclusion of the term $\frac{\partial u^*}{\partial t}$ in (6)

2. the coriolis terms are of the form $(\bar{u} - u^*) \cdot f$ instead of $(\bar{u} - u_g) \cdot f$. We are using the actual background wind instead of the geostrophic wind.

It is also seen that in steady state conditions $\frac{\partial u^*}{\partial t} = 0$ so that (6) and (8) are almost identical but for $u_g \to u^*$. This means that they behave mathematically similarly in the steady case. The inclusion of the term $\frac{\partial u^*}{\partial t}$ and the replacement of u_g by u^* have, however, fundamental consequences, which will be discussed in the next section.

3 Filtering of inertial-diffusive oscillations

Ching & Businger (1968) solved the Ekman boundary layer equations (8) with constant K and with a rotating pressure gradient given

by a time variation of the geostrophic wind according to

$$(9) \qquad \mathbf{V}_g(t) = u_{go} e^{i\alpha t} , \qquad \mathbf{V}_g = u_g + i \cdot v_g$$

For α corresponding to a period of rotation of 24 hours the solution exhibited very marked inertial oscillation. Fig 2 shows a corresponding numerical integration, but with the variable K described below. The wind hodographs in fig 1 look very similar to the ones obtained by Ching & Businger. The amplitude of this oscillation is quite large but decreases with the rotational speed of the pressure gradient. Even if these inertial oscillation might be essential in some cases, for example as a contributing factor in explaining the nocturnal jet of the Great Plains in U S A, where f and α (30°N) are of about the same size, it seems that these inertial oscillations, depending on variable pressure gradients, are not observed in northern latitudes (~ 50° - 60°N) and are probably overshadowed by other processes. (See for example Peagle & Rasch(1973), Young (1973)). It seems therefore to be desirable to filter out these inertia-oscillations. This is in fact done by the formulation (6). Inertial oscillations are not, however, completely excluded from the model. The large scale equations are still capable of taking care of inertial oscillations to the extent that they exist in the large scale model, and are introduced by means of the boundary conditions $u' = - u^*(t)$, $v' = - v^*(t)$ at $z = z_0$. A test run was made with the equations (6) with the same variation $\mathbf{V}$ as used for $\mathbf{V}_g$ in the Ching & Businger case. No inertia-oscillations were present.

We can also see this clearly if we assume the background flow to be defined by

$$(10) \qquad \begin{cases} \dfrac{\partial u^*}{\partial t} - f(v^* - v_g) = 0 \\[2ex] \dfrac{\partial v^*}{\partial t} + f(u^* - u_g) = 0 \end{cases}$$

and $\mathbf{V}_g$ given by (9).

Eq (10) can only describe an adjustment between the wind and the massfield by means of inertial oscillations.

We also have from eq (6)

$$(11)\quad \begin{cases} \dfrac{\partial \bar{u}}{\partial t} - \dfrac{\partial u^*}{\partial t} - f(\bar{v} - v^*) = \dfrac{\partial}{\partial z}\left(K'_m \dfrac{\partial u'}{\partial z}\right) = \dfrac{\partial}{\partial z}\left(K'_m \dfrac{\partial \bar{u}}{\partial z}\right) \\ \dfrac{\partial \bar{v}}{\partial t} - \dfrac{\partial v^*}{\partial t} + f(\bar{u} - u^*) = \dfrac{\partial}{\partial z}\left(K'_m \dfrac{\partial u'}{\partial z}\right) = \dfrac{\partial}{\partial z}\left(K'_m \dfrac{\partial \bar{v}}{\partial z}\right) \end{cases}$$

adding (10) gives

$$(12)\quad \begin{cases} \dfrac{\partial \bar{u}}{\partial t} - f(\bar{v} - v_g) = \dfrac{\partial}{\partial z}\left(K'_m \dfrac{\partial \bar{u}}{\partial z}\right) \\ \dfrac{\partial \bar{v}}{\partial t} + f(\bar{u} - u_g) = \dfrac{\partial}{\partial z}\left(K'_m \dfrac{\partial \bar{v}}{\partial z}\right) \end{cases}$$

which is the set of eq (8) above. We thus see that in this simple case we have just subtracted the inertial motion from our boundary layer equations and instead placed it in the large scale flow equations. In order then to get inertia-oscillations as a solution to (6) we must solve equations (10) with $\mathbf{V}_g = u_{go} e^{i\alpha t}$ and the initial conditions $u^* = u_{go}$, $v^* = 0$ for $t = 0$. The proper time variation in u^*, v^* is then given by the solution

$$(13)\qquad w^* = u^* + i \cdot v^* = u_{go}\left[\left(1 - \frac{f}{\alpha+f}\right)e^{-ift} + \frac{f}{\alpha+f}\, e^{i\alpha t}\right]$$

The equations (6) were solved with this boundary condition instead of $\mathbf{V}^* = u_{go} e^{i\alpha t}$ and gave, as expected, exactly the same solution as (8).

Our boundary layer equations therefore have the desirable property of filtering out inertial oscillations due to time variations in the pressure gradient, which are enchanced when $\alpha \sim f$.

4 Formulation of K for neutral and stable stratification

The turbulent coefficient used in this study is based on

1. An extension of the exchange coefficient for neutral conditions in the constant flux layer to include the whole boundary layer. This is done by means of a reduction in mixing length ℓ which is due to Blackadar (1962).

2. A stability dependence using Monin -Obukhov's similarity theory. The present form of K is suggested by Karlsson (1972).

K_m is then expressed as

$$(14) \qquad K_m = \frac{\kappa^2 z^2}{(1+\frac{\kappa z}{\lambda})^2} \cdot \frac{1}{(1+\alpha Ri)^2} \left|\frac{d\mathbb{V}}{dz}\right|$$

where

$$(15) \qquad Ri = \frac{g}{T} \cdot \frac{(\frac{\partial T}{\partial z} + \Gamma)}{\left|\frac{d\mathbb{V}}{dz}\right|^2} = \text{Richardson Number}$$

Γ = adiabatic lapse rate (dry or moist)

κ = von Karmans constant taken as 0.4

(measurements by Businger et. al. (1971) indicate that κ instead is equal to 0.35)

$$(16) \qquad \lambda = \mu \cdot \frac{G}{f} \qquad \text{where} \qquad G = (u_g^2 + v_g^2)^{1/2}$$

and $\mu = 3 \cdot 10^{-4}$

$\alpha = 3.0$

In this case u_g and v_g are replaced by u^* and v^*.

The mixing length is then taken as

$$(17) \qquad l = \frac{\kappa z}{1+\frac{\kappa z}{\lambda}}$$

with $\lim_{z \to \infty} l = \lambda$

The eddy coefficient for heat exchange is given by $K_H = \frac{K_m}{1+\alpha \cdot Ri}$

The assumption that λ only depends on geostrophic wind is however a weak point. l should in some way depend on stability, as for example suggested by Delage (1973). The form (17) was suggested by Blackadar for neutral conditions. This is however not crucial

for the present study where the aim has been to study the problems and effects of large scale forcing, i.e. variations in time of background wind and temperature. A new parameterization of the turbulent exchange in the boundary layer will be adopted in the future work. This formulation is suggested by Deardorff (personal communication) and follows essentially Delage for the stable case and employs the results from Deardorff (1972, 1973) for the unstable boundary layer. It also uses the equation for turbulent energy instead of an explicit formulation for K.

5 Numerical solution

5.1 The equations (6) are approximated by means of finite differences in space and time. In the z-direction an expanding grid is used. The strongest gradients are found in the lowest 20-30 m of the boundary layer and it is therefore convenient to have the highest resolution in the bottom layer. If we denote $\Delta Z_1 = Z_1$ and $\Delta Z_i = Z_i - Z_{i-1}$ and assume a constant ratio

$$k = \frac{\Delta Z_{i+1}}{\Delta Z_i}$$

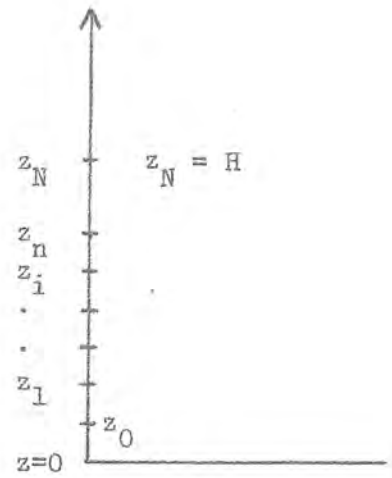

we can write the heights to the gridpoints

$$Z_n = \Delta Z_1 \frac{k^n - 1}{k - 1} \qquad (18)$$

$$n = 0, 1, 2, \ldots\ldots\ldots\ldots N$$

The top of the computational boundary layer, H , is usually 1 500 m. The lowest gridpoint is not, however, Z = 0 but $Z = Z_0$, where the boundary conditions are applied. In most of the computations 100 points (k = 1.0555) have been used which almost completely elminates the error introduced by making the centered finite differences slightly "uncentered" because of (18). In fact experiments have shown that this grid can be used successfully down to the order of 40 gridpoints (k = 1.1823), $Z_0 \leq Z \leq 1500$, without any noticeable errors. The solution has then been compared with the case where the vertical coordinate Z has been transformed to a new one, y , by means of

$$(19) \qquad Z = a \cdot \frac{K^y - 1}{K-1} \quad \text{or} \quad y = \frac{1}{\log K} \log\left(\frac{K-1}{a} \cdot Z + 1\right)$$

y has been discretized into equividistance points. No significant differences were found for $N \geq 30$ points. It should be pointed out that this is applicable only to the stable or neutral BL, where K is fairly small.

5.2 For the numerical time integration a Crank-Nicolson scheme has been used. If we write the first equation of motion as

$$\frac{\partial u}{\partial t} = F + f \cdot v \qquad \text{where} \qquad F = \frac{\partial}{\partial z}\left(K \frac{\partial u}{\partial z}\right)$$

we get

$$(20) \qquad \frac{u_j^{n+1} - u_j^n}{\Delta t} = \theta \cdot F_j^{n+1} + (1-\theta) F_j^n + f \cdot v_j^n$$

where

$$(21) \qquad F_j^n = \frac{K_{j+1/2}^n \dfrac{u_{j+1}^n - u_j^n}{z_{j+1} - z_j} - K_{j-1/2}^n \dfrac{u_j^n - u_{j-1}^n}{z_j - z_{j+1}}}{\dfrac{z_{j+1} - z_{j-1}}{2}}$$

With $K^{n+1} = K^n$ in (20) we obtain a set of linear equations in u_j to be solved. In (20) the Crank-Nicolson scheme is stable if $\theta \varepsilon (1/2, 1)$ (Richtmeyer & Morton) However, the coriolis term, which

is treated explicitly, grows slowly, but with a time-step about 30 sec there are no problems. Treating the coriolis term explicitly simplifies the numerical procedure quite a lot. An improvement would be of course to use some type of multistep method for this term, e.g. Adams-Bashforth. Eq (6 b) and (6 c) are treated in a similar way. The sets of linear equations are solved by means of Gauss´elimination.

Due to the formulation of K, where K is proportional to $|\frac{\partial v}{\partial z}|^5$, the equations (6) are highly non-linear. This resulted in non-linear instability in the first runs. To avoid this non-linear instability a time smoothing in K was applied according to

$$\bar{K}^t = (K^t + 2\,K^{t-1} + K^{t-2})/4 \qquad (22)$$

This remedied the non-linear instability.

During most of the computations 100 gridpoints between z = 0 and z = 1 500 m have been used but in the later cases only 70 gridpoints. The timestep has been 30 seconds.

5.2 Initialization

In most experiments the integration has started form a steady-state windprofile $\mathbf{V}_s(z)$ satisfying

$$\frac{\partial}{\partial z}\left(K'_m \frac{\partial u_s}{\partial z}\right) + f v_s = 0$$

$$\frac{\partial}{\partial z}\left(K'_m \frac{\partial v_s}{\partial z}\right) - f \cdot u_s = 0 \qquad (23)$$

with K'_m as in (14). Initial values for T' have been used in the Richardson number and an iterative technique has then been used in solving (23), giving a K'_m-profile and $u_s(z)$, $v_s(z)$ which are consistent with each other. In this case the two equations had to be solved simultaneously. The procedure takes about 50 iterations to converge when starting from an Ekman spiral. However, this method is considerably more efficient than a time integration to a steady-state. In some integrations we have started from different initial conditions, i.e. not initialized in order to study

the effect and influence on the solution from variations in the initial data. This is of course an essential problem since in reality we can expect fairly large errors in the input data for the model, especially as regarding wind data. This will be studied in some more detail in future work.

6 Heat conduction in the soil and heat flux at the earths´surface

When trying to model the atmosphere boundary layer it is essential to include the heat transfer across the earths´ surface to calculate the energy balance due to in- and outgoing radiation, turbulent heat flux and heat flux from the soil. Even early boundary layer models (Estoque, 1963, Pandolfo et al,1965) as well as more recent ones (Sasamori, 1970, Zdunkowski & Barr, 1972) have an equation for heat conduction in the top soil layer in order to get the surface heat flux from the ground. Usually a fairly crude approximation of the heat flux has been used, partly due to a lack of knowledge of specific soil characteristics and their vertical distribution. Generally the boundary layer models use horizontal averages of z_0 as well as specific heat (c_s) and heat conductivity (λ) in the soil. But both c_s and λ depend on moisture content in the soil in a complicated way. Due to lack of more detailed knowledge of these properties vertically, constant values for c_s and λ have been used which reduces the heat conduction equation to the simple form

$$(24) \qquad \frac{\partial T}{\partial t} = K_s \frac{\partial^2 T}{\partial z^2}$$

where the thermal conductivity

$$K_s = \frac{\lambda}{c_s}$$

This is the ordinary parabolic diffusion equation. In most cases (24) has been solved numerically be means of finite differences in space and time. However, it seems that the numerical technique involves a number of superflous computations considering the poorly known initial state of the soil temperature and the simplifying assumptions behind (23). Instead it should be possible to

use a simple fourier series solution by means of which the heat flux, H(t), is calculated from knowledge of the surface temperature $T_0(\tau)$, $0 \leq \tau \leq t$.

Assume a soil layer of depth D, below which the temperature does not change

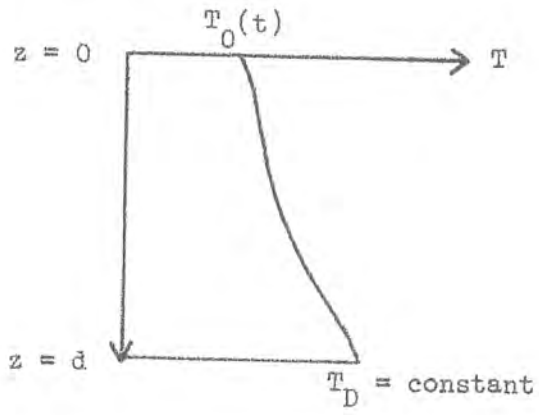

and a surface temperature $T_0(t)$. Initially the temperature distribution is g(z). We then have to solve eq (24) with the boundary and initial conditions

$$
\begin{aligned}
&T = T_D && z = D \\
&T = T_0(t) && z = 0 \\
&T = g(z) && t = 0
\end{aligned}
\tag{25}
$$

A classical solution to this problem is (see for example Carslaw, 1921)

$$
T(z,t) = T_D + \frac{T_0 - T_D}{D}(D - z) + \frac{2}{D}\sum_{n=1}^{\infty} e^{-\frac{n^2\pi^2 K_{st}}{D^2}} \sin\frac{n\pi}{D} z \int_0^D h(z') \sin\frac{n\pi}{D} \cdot Z' dz' - \frac{2}{\pi}\sum_{n=1}^{\infty}\frac{1}{n} e^{-\frac{n^2\pi^2 K_{st}}{D^2}} \sin\frac{n\pi}{D} z \int_0^t \frac{\partial T_0}{\partial t'} e^{\frac{n^2\pi^2 K_{st'}}{D^2}} dt \tag{ }
$$

where

$$
h(z) = g(z) - \frac{T_D - T_0(0)}{D}(z - D) - T_D
$$

that is we have subtracted an initial linear profile.

Eq (26) can also be rewritten by means of a partial integration of the time integral.

In most cases it seems extravagant to assume anything more than an initially linear profile g(z)

$$(27) \qquad g(z) = T_D + \frac{T_0(0) - T_D}{D}(D - z)$$

In that case the second term in eq (26) vanishes. The heat flux is then computed by forming

$$H = - C_s K_s \left(\frac{\partial T}{\partial z}\right)_{z=0}$$

In order to approximate the time integral we introduce a time step Δt so that $t_j = j \cdot \Delta t$, $j = 0, 1, 2, \ldots\ldots$

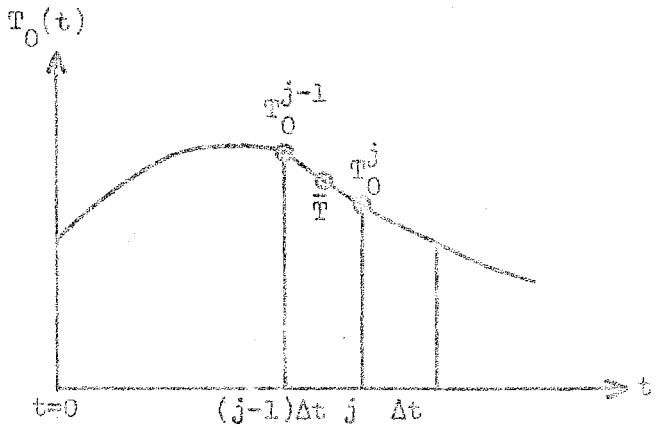

and put $\left(\frac{\partial T_0}{\partial t}\right)_{t=j\Delta t} = \frac{T_0^j - T_0^{j-1}}{\Delta t}$

In the rewritten version an average value of T is used in the interval

$$(j-1)\Delta t < t < j \ \Delta t \qquad \bar{T} = \frac{T_0^j + T_0^{j-1}}{2}$$

The time integral in eq (26) can then be written as

$$(28)\qquad \int_0^t \frac{\partial T_0}{\partial t'} e^{\alpha n^2 t'} dt' = \sum_{i=1}^{j} \int_{(i-1)\Delta t}^{i\Delta t} \frac{T_0^i - T^{i-1}}{\Delta t} e^{\alpha n^2 t'} dt' =$$

$$= \sum_{j=1}^{j} \frac{T_0^{i-1} - T_0^i}{\alpha n^2} e^{i\alpha n^2 \Delta t} \left(1 - e^{\alpha n^2 \Delta t}\right)$$

and correspondingly for the rewritten version.

Finally

$$(29.1)\quad H_1 = C_s K_s \left\{ \frac{T_0(j\Delta t) - T_D}{D} + \frac{2}{\mu} \sum_{n=1}^{N} \frac{1}{n^2} \left(e^{-\mu n^2 j} - e^{-\mu n^2 (j+1)} \right) \cdot \right.$$

$$\left. \left(\sum_{i=1}^{j} (T_0^i - T_0^{i-1}) e^{in^2 \mu} \right) \right\}$$

$$(29.2)\quad H_2 = C_s K_s \left\{ \frac{T_0(0) - T_D}{D} - \frac{2}{D} \sum_{n=1}^{N} \left(e^{-\mu j n^2} - e^{-\mu n^2 (j+1)} \right) \right.$$

$$\left. \sum_{i=1}^{j} \left(\frac{T_0^i + T_0^{i-1}}{2} \right) e^{i\mu n^2} \right\}$$

where H_1 is the flux according to eq (26) and H_2 according to the partially integrated version. We have further truncated the series expansion at n = N. The sums involving T_0 can be accumulated from time step to time step and only involves adding extra terms for each new time step. The convergence rate is however important in comparing the efficiency of this method with the ordinary finite difference methods. The first results have not been encouraging in this respect showing a fairly slow convergence, both for (29.1) and (29.2) and a dependence of the convergence rate on the depth of the soil layer D.

Shaffer & Long (1973) have recently suggested another form for the analytical solution which seems to be very efficient. They adopt the lower boundary condition at infinity:

$$T \to \text{constant}, T_\infty, \; z \to \infty$$

and get a Greens function solution which involves no series expansion.

They do not discuss, however, the effect of this other boundary condition on the solution for H or the accuracy as compared with the finite difference solution.

The two equations (29.1) and (29.2) as well as a corrected version of Shaffer & Longs formulation have been tested together with a finite difference analogue to eq (23) with a simple explicit time integration. The variation of $T_0(t)$ has been given by

$$T_0(t) = 283.0 + 10 \cdot \sin\left(\frac{2\pi t}{p} - \alpha\right)$$

p = 24 hours

α = corresponds to a phaseshift of 7 hours. (α=1.8325)

i.e. a temperature maximum at 1300 hours.

In the finite difference formulation a logarithmic vertical coordinate has been used. Fig 3 summerizes some of the results from the test runs. It shows that neither ( ) nor ( ) gives satisfactory results. The Shaffer & Long formulation seems to give a fairly good result, especially for large fluxes. In the application of Shaffer & Longs formulation the initial linear temperature profile between z = 0 and z = D has been extended by means of an exponential function of z. The linear part of the initial profile adds some extra error functions to be evaluated at each time step, which makes the computation quite time consuming.

7 Results of numerical integrations

A number of experiments have been carried out to test the behaviour of the PBL-model for assumed variations in background wind and temperature. Some of them have only been run to be able to compare them with other authors' results as a check on the gross properties of the model and the accuracy of the numerical formulation. This includes experiments with rotating but constant pressure gradient/background wind, sudden change of

roughness height (P A Taylor, 1969) and variation of windspeed but not direction (Lykosov, 1972).

In all the experiments the background temperature has been constant. The lower and upper boundary conditions for T' have been T = 0.

7.1 A very important problem today is the parameterization of the boundary layer in large scale numerical models. In the resistance law formulations the stress (in fact u_*) and the angle between the geostrophic wind and the surface wind are computed from a matching of an inner logarithmic surface layer and an outer Ekman layer. The theory has also been generalized to include a stability dependence. This is achieved by fitting the two constants, A and B, as functions of a bulk Richardson number or the Monin-Obukhov length to observations. In the theory, however, the boundary layer is assumed to be in a steady state. In Melgorejo & Deardorff (1974), using a formulation of the resistance law according to Deardorff & Zilitinkevich (1974), the constants A and B are determined from the Wangara data set (Clarke et al 1971). An interesting feature in the results is the large scatter in the values in stable region, which also has been present in earlier evaluations. In the experiments carried out in this study friction velocity, u_*, and the angle between the background, large scale wind, and the surface wind (deviation) have been computed. In addition the corresponding steady state u_* and deviation with the same background winds as in the unsteady model have been computed. The differences between steady and unsteady computations are most striking for the deviation angle as will be seen below. These tentative results seem to indicate that the unsteadyness in the large scale flow is a contributing factor in determining the stress and crossisobar flow near the surface and a possible explanation to the large scatter obtained when fitting the resistance low constants to observations in the stable range.

7.2 The first experiment is basically the same as in Lykosov (1972). The background wind $\mathbf{V}^*$ is given by

$$u^* = 10.0 - 10.0 \cos\left(\frac{2\pi}{T}(t - t_1)\right)$$

$$v^* = 0.0$$

$$T = 24 \text{ h}$$

i.e. the background wind starts at roughly 20 m/s, decreases to zero and increases back again to 20 m/s, The background temperature, T^*, is constant with height, equal to 283.0 K. Roughness height is z_0 = 0.01 m. Fig 3 and 4 show wind hodographs for each third hour. The initial wind profile is obtained by means of the initialization procedure in paragraph 5.2. The most striking feature is the shape of the wind hodographs after 15 hours. The background wind is then approximately zero but there is still a momentum transport going on in the boundary layer showing the slow response to changes in the background flow. The hodographs after 19 and 22 hours show a spiral form and a kink at about 300 m when the background wind forces an adjustment to an Ekman type of hodograph. Large variations in the cross isobar angle are also seen. This is more obvious in fig 6, which shows the deviation angle and the friction velocity as a function of time. Both are calculated at z = 2 m. The deviation angle exhibits large variations with time with an oscillation present after the background wind has started to increase again. u_* has a much more regular behaviour being basically proportional to the background wind. The dashed curves show the corresponding deviation angle and u_* from steady state computation. The deviation angle is fairly constant over all the 24 hours. While the steady state u_* follows the unsteady u_* quite well with an error generally about 10 % the differences between the two deviation angles are huge. This is not so surprising for very weak background winds but even for a background wind amounting to 10 m/s the steady state deviation angle is only 50 % of the unsteady state one.

Fig 5 shows three profiles of the eddy exchange coefficient, K. No upper boundary conditions of zero flux at the top of the boundary layer is applied, but K vanishes nicely already at about 900 m in this case. The height of maximum K decreases from about 125 m to 70 m after 9 hours when the background wind is about 7.5 m/s.

7.3 The second experiment deals with a problem of a sudden change both in wind direction and wind speed. This can be thought of as for example the passage of a through line or a front. The initial background wind is westerly, 5 m/s. The model is ini-

tialized and then the background wind suddenly changes to a southerly direction and increases to 15 m/s. The background temperature is given by $T^* = 283.0 - 0.005 \cdot Z$, Z is height. $T' = 0$ at the upper and lower boundary, $Z_0 = 0.01$ m. Fig 7 shows the results. After 5 minutes there is a very marked internal boundary layer where all the shear is concentrated to the lowest 25 m. With increasing time there is a slow and gradual adjustment to a steady state generalized Ekman profile, but not even after 5 hours has a steady state been achieved. The corresponding deviation angle and u_*, both from the unsteady and steady state, are shown. Deviation and u_* oscillate considerably approaching asymptotically the steady state values. The error in u_*, disregarding the first 30 minutes, is at a maximum after 2-3 hours amounting to about 20 %.

7.4 The last experiment reported on here deals with a rotating wind which at the same time decreases linearly. The background wind is described by

$$u^* = |\mathbb{V}^*| \cos \alpha t$$

$$v^* = |\mathbb{V}^*| \cdot \sin \alpha t$$

$$|\mathbb{V}^*| = 15 - 10 \cdot \frac{t}{12 \text{ h}}$$

Background temperature $T^* = 283.0 - 0.005 \cdot Z$

$Z_0 = 0.01$ m

$T' = 0$ at $Z = Z_0$ and $Z = H$

α corresponds to a period of 24 hours. In this experiment the model has been run with three different initial wind-distributions in the vertical.

1. Wind profile from the initialization procedure
2. Ekman profile with constant K
3. $u = 15 \cdot \frac{Z}{H}$

   $v = 0.0$

Fig 9, 11 and 13 show the wind hodographs corresponding to 1., 2. and 3. It is obvious that the different initial conditions have a marked influence on the result. However, the constant flux layer seems to be well established and the largest diffe-

rences are found above ~ 50 - 100 m. Of course the third case is rather absurd and shows large differences from the other two cases. Fig 10, 12 and 14 show the deviation angles as well as u_* from the unsteady and steady cases. In the initialized case in fig 11 the differences in deviation angle is not so pronounced as in the former experiments while u_* differs with about 10 - 15 %. Of course the differences increase in the other two cases.

This shows that in stable stratification in the boundary layer the adjustment time due to turbulence is fairly long leading to a strong dependence in the solution on the initial wind distribution. On the other hand this also means that in unsteady conditions it is risky to use initialized steady state profiles as initial conditions. How this is going to be solved in practice is a difficult question.

Finally, fig 15 shows two K_m-profiles, one after 6 hours and another after 12 hours. The behaviour is very regular with a maximum at 100 m after 6 hours which goes down to 45 m after 21 hours when the background wind speed is only 5 m/s.

8 Conclusions and discussion

This study, which is the first part in an effort to develop an operational atmospheric boundary layer model, has shown the feasability of using Gutmans approach in formulating a one-dimensional boundary layer model. It has also been demonstrated that this formulation filters out inertial-diffusive oscillations due to unsteadyness in the pressure field. This property gives the model certain advantages as compared with the usual Ekman formulation.

The use of the Crank-Nicolson scheme seems to be a natural and efficient choice when dealing with diffusion problems. The rather ad hoc introduction of a time smoothing of K is probably possible to get rid of when turning to the new turbulence formulation using a turbulent energy equation for closing the set of equations.

The first simple experiments with a stably stratified boundary layer model with unsteady large scale background flow show very big and marked differences as compared with steady state solutions.

A comparison between the angle between the surface wind and the background wind and friction velocity u_* from the unsteady computations and from corresponding steady states has been made. This comparison shows that the differences in u_* rarely exceeds 15% but that there are big differences in the deviation angles amounting to up to 100%. This indicates a possible explanation for the large scatter when fitting the resistance law constants to observations in the stable range.

Finally an attempt has been made to use an analytical fourier solution to the heat conduction equation in order to calculate the heat flux through the earths´surface. This solution has been compared with a finite difference solution with very high accuracy and with an analytical solution due to Shaffer & Long using Green´s function. The results indicate that the Shaffer & Long method (after corrections) gives the best results even if it not coincides with the true solution. However, that solution is not as efficient as claimed by Shaffer & Long, after the corrections have been introduced.

Next in line is the introduction of a more realistic description of turbulence in the model as well as the introduction of radiation, a soil layer and an energy balance equation at the ground. Later moisture will be introduced and the model run with real background data as well as initial data.

Acknowledgements

The author is indebted to Dr I Holmström for many valuable suggestions and kind support. The author also wishes to thank Mr H Basun, Mr A Forsberg and Mr B Karlsson for programming aid, Mrs Wera Böhm for drawing the figures and Mrs Barbro Tvetström for typing the manuscript. Finally a thank to Professor Gutman for discussions of the basic ideas in formulating atmospheric boundary layer model during a visit to Novosibirsk Computing Center in 1971.

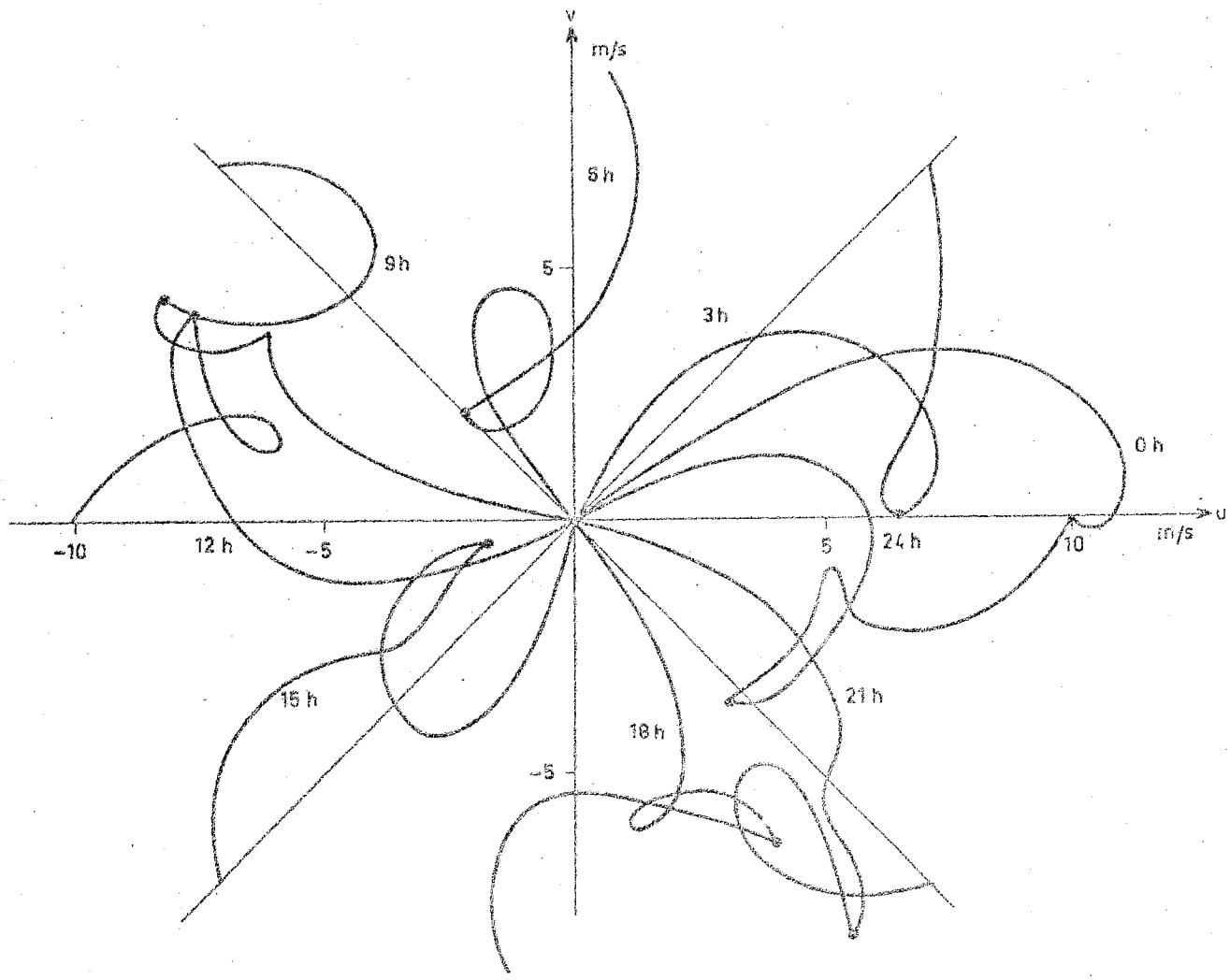

Fig. 1 Wind hodographs computed from ordinary Ekman layer equations. The eddy coefficient is the one described in the text but the temperature has been kept constant in time and space. The geostrophic wind vector rotates with one revolution in 24 h with constant magnitude, 10 m/s. Z_0 = 0.1 m and the computational top of the model is at H = 1 500 m. The dots mark the height 535 m.

Vindhodografer som beräknats från Ekman-skiktsekvationer. Den turbulenta utbyteskoefficienten är den som beskrivits i texten. Temperaturen har dock hållits konstant, både i tiden och rummet. Den geostrofiska vindvektorn roterar ett varv på 24 timmar med konstant styrka, 10 m/s. Z_0 = 0.1 m och den översta nivån i modellen ligger på H = 1 500 m. Punkterna markerar höjden 535 m.

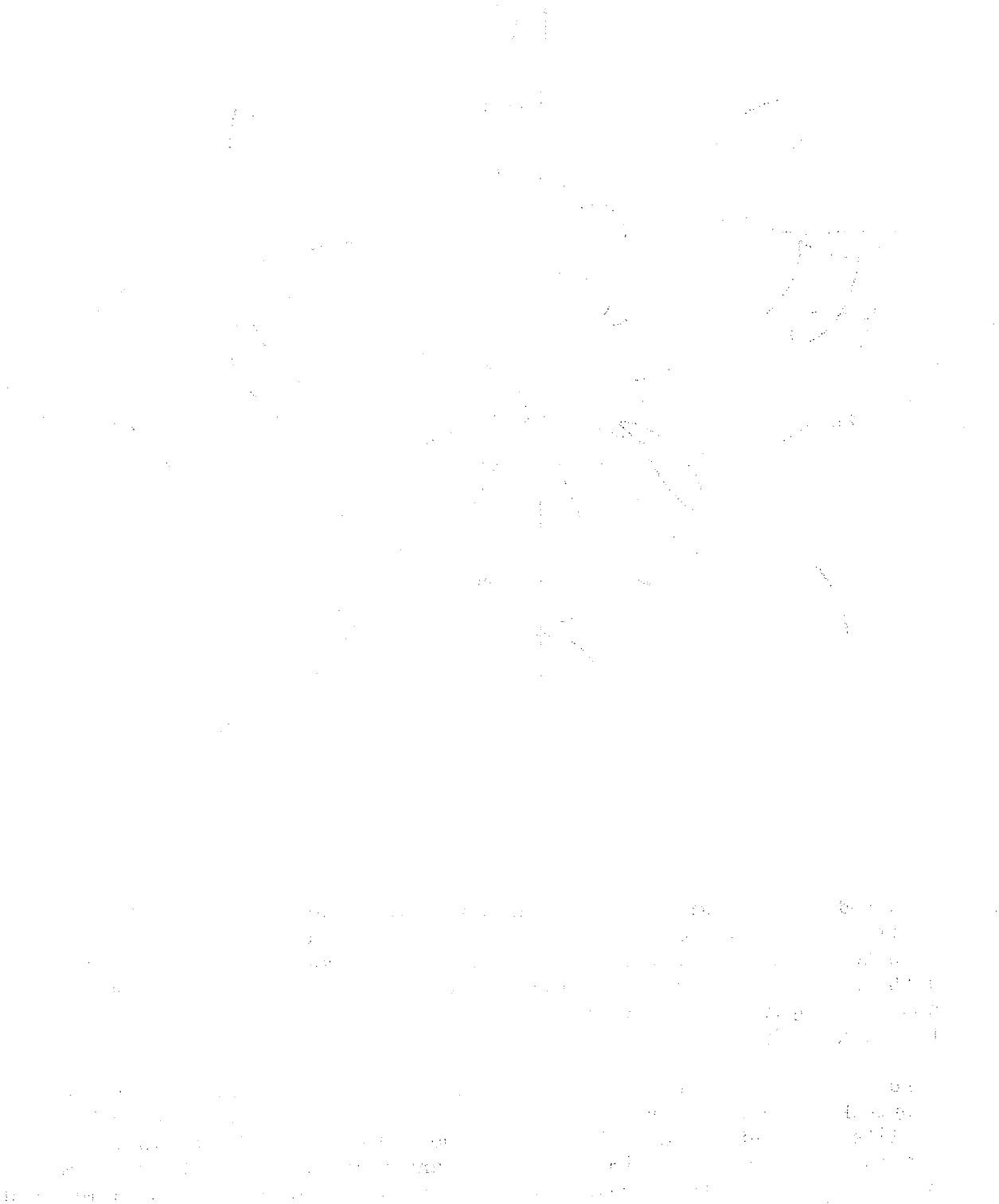

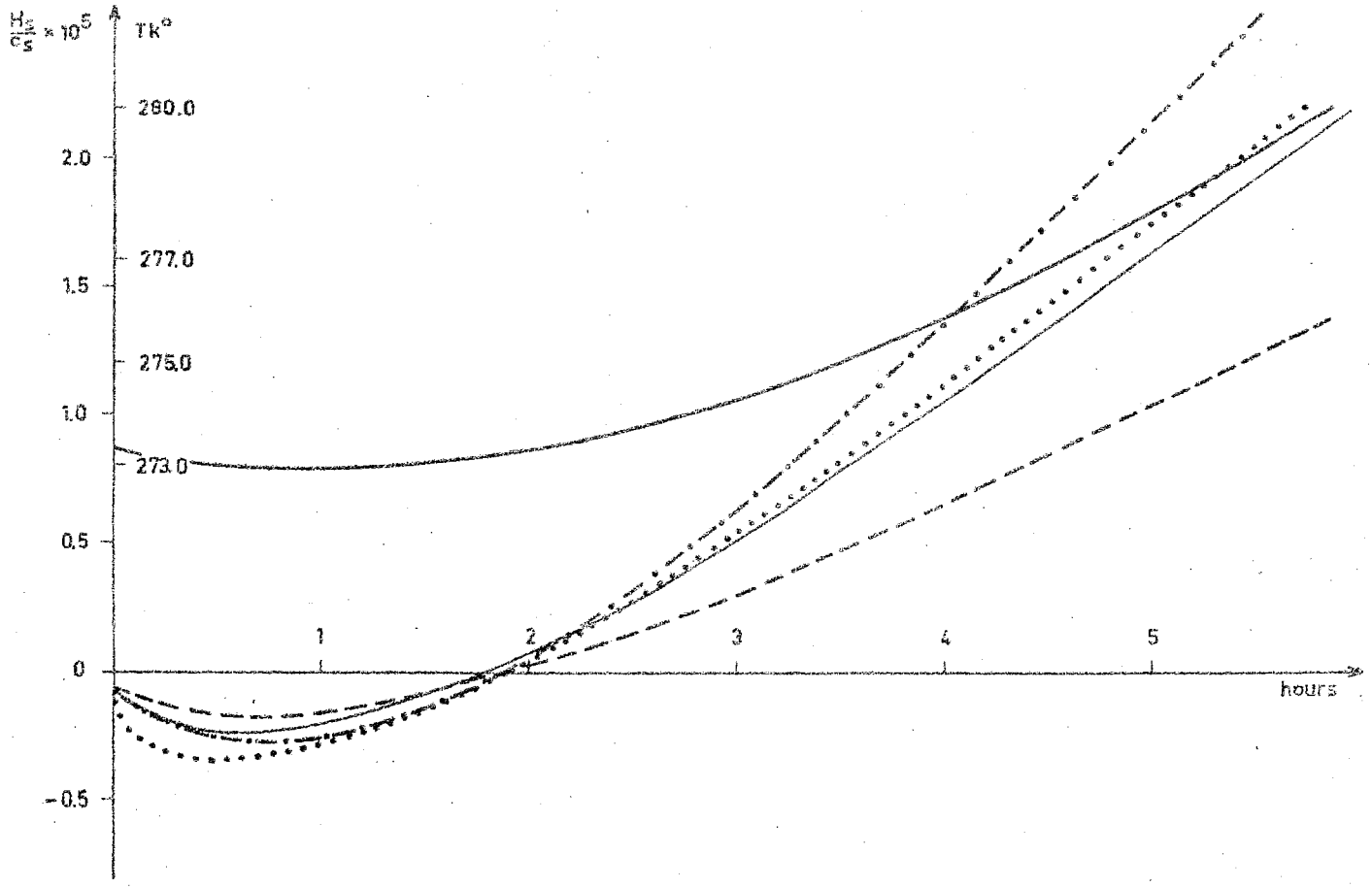

Fig. 2 Summary of heat fluxes as a function of time computed from different solutions of the heat conduction equation. The heavy full curve shows the assumed surface temperature as a function of time. The thin full line shows the high accuracy, finite differences solution. Dashed and dashed-dotted curves show heat fluxes obtained from the fourier solutions according to eq. (29.1) with depth 0.64 m and 1.5 m respectively. In both cases 50 terms are included in the series. Finally the dotted curve shows the heat flux according to the corrected Shaffer & Long method.

Sammanställning av värmeflöden som funktioner av tiden beräknade från olika lösningar till värmeledningsekvationen. Den tjocka heldragna kurvan visar den antagna variation av marktemperaturen som funktion av tiden. Den tunna heldragna kurvan visar resultatet från en finit-differenslösning med stor noggrannhet. De streckade och streck-prickade kurvorna visar värmeflöden som erhållits från ekvation (29.1) med repektive djupet 0.64 m och 1.5 m. I bägge fallen har 50 termer använts i serien. Slutligen visar den prickade kurvan värmeflödet enligt den korrigerade Shaffer & Longs metod.

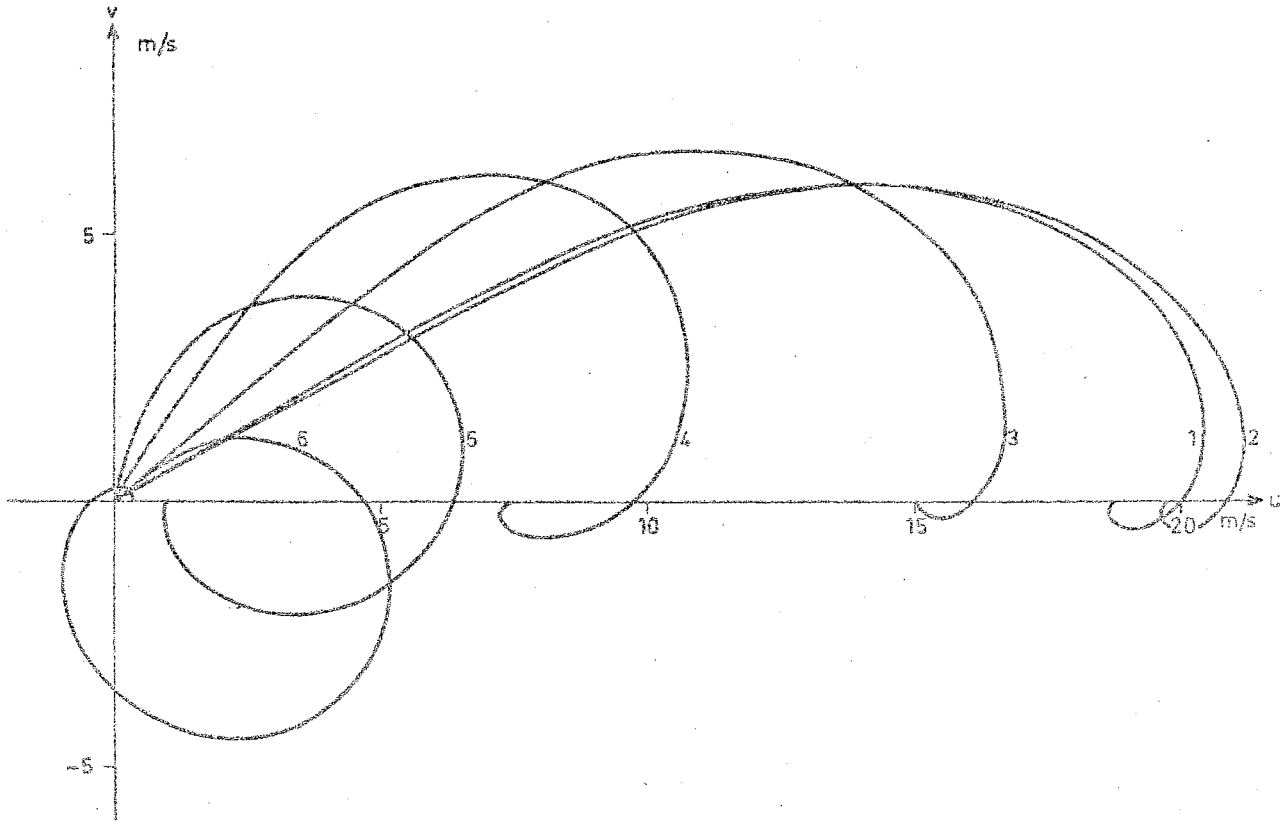

Fig. 3 Wind hodographs computed by the model devloped in this study. The background wind variation is given by

$$v^* = 0$$
$$u^* = 10.0 - 10.0 \cos\left(\frac{2\pi}{T}(t - t_1)\right)$$

where $T = 24$ h
$Z_0 = 0.01$ m, $T^* = 283.0$ K for all Z.
The wind hodographs correspond to
1. t = 0 h, 2. 3h, 3. 6 h, 4. 9 h, 5. 12 h and 6. 15 h.

Vindhodografer beräknade med den här utvecklade modellen. Bakgrundsvinden ges av

$$v^* = 0$$
$$u^* = 10.0 - 10.0 \cos\left(\frac{2\pi}{T}(t - t_1)\right)$$

där $T = 24$ t
$Z_0 = 0.01$ m, $T^* = 283.0$ K för alla Z.
Vindhodograferna visas efter
1. t = 0 t, 2. 3 t, 3. 6 t, 4. 9 t, 5. 12 t och 6. 15 t.

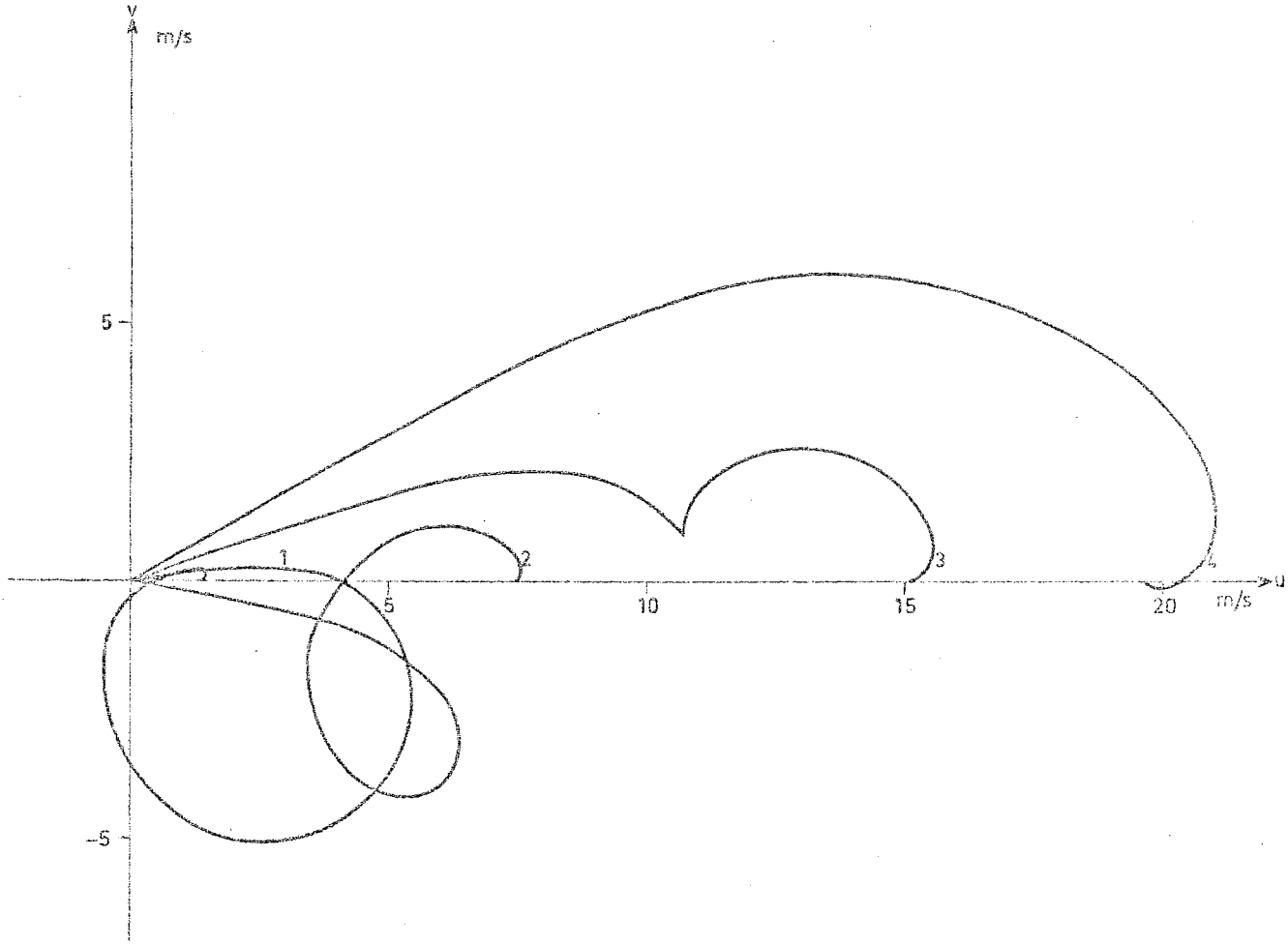

Fig. 4 The same as for fig. 3 but after
1. t = 16 h, 2. 19 h, 3. 22 h and 4. 25 h

Samma som för fig 3 men efter
1. t = 16 t, 2. 19 t, 3. 33 t och 4. 25 t

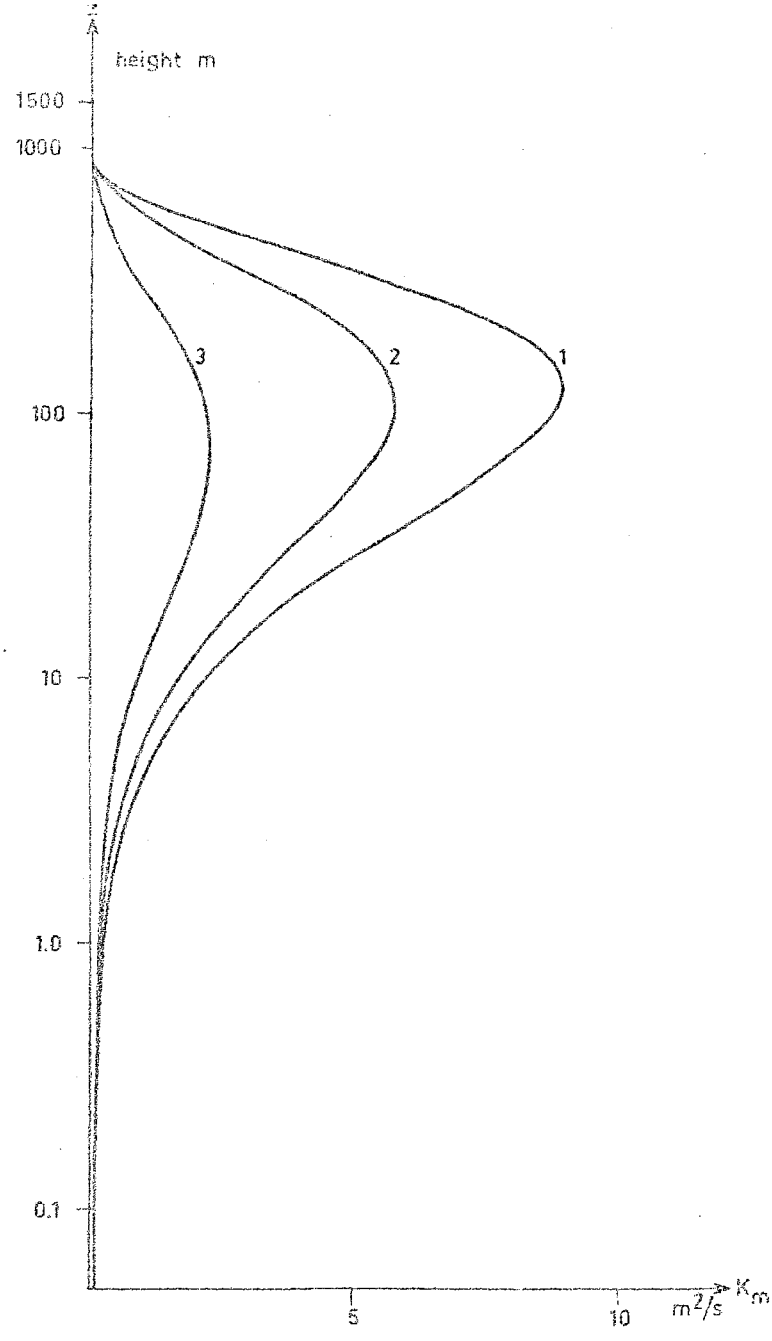

Fig. 5 Profiles of the eddy exchange coefficient after 1. t = 3 h, 2. 6 h and 3. 9 h. Background wind as in fig. 3

Profiler för den turbulenta utbyteskoefficienten efter 1. t = 3 t, 2. 6 t och 3. 9 t. Samma bakgrundsvind som i fig 3

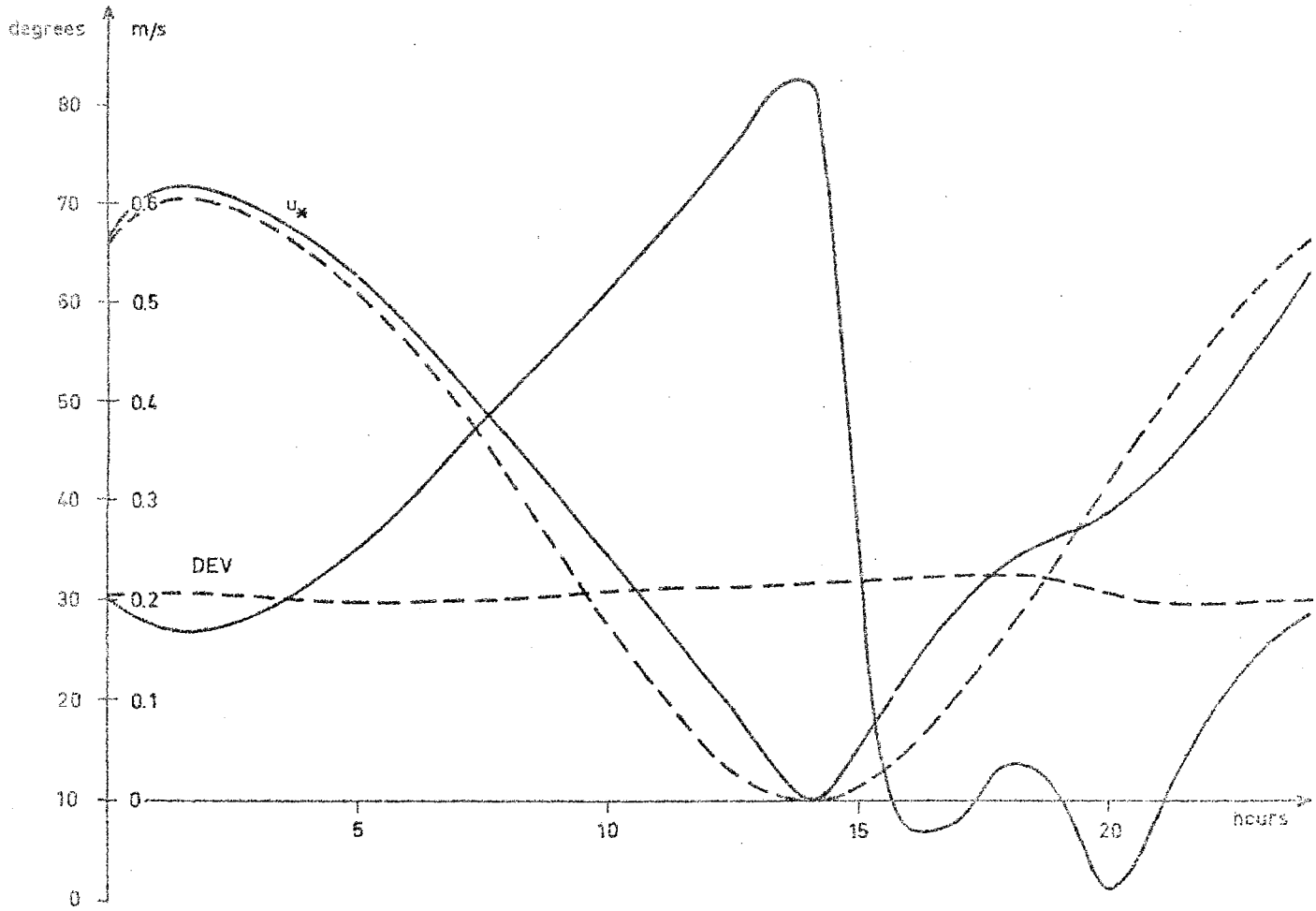

Fig. 6 Friction velocity and surface wind deviation angle as a function of time. Background wind as in fig. 3. Dashed curves show the corresponding steady state u_* and deviation angle for the same background wind.

Friktionshastighet och avvikelsen mellan markvind och bakgrundsvind som funktion av tiden. Bakgrundsvinden samma som i fig 3. Streckade kurvor visar motsvarande stationära u_* och vinkelavvikelse för samma bakgrundsvind.

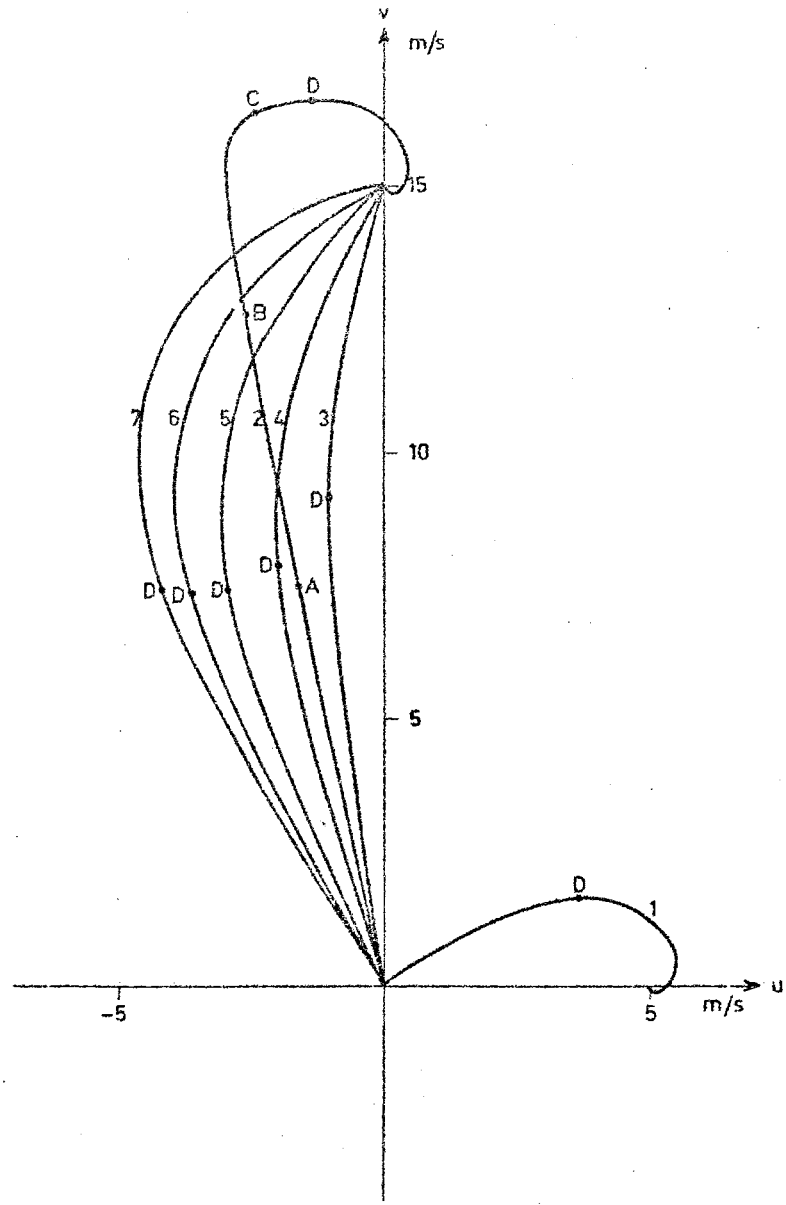

Fig. 7 Wind hodographs. The background wind is initially $u^* = 5$ m/s, $v^* = 0$. The model is initialized and then the background wind suddenly changes to $u^* = 0$, $v^* = 15$ m/s. In the run $Z_0 = 0.01$ m, $T^* = 283.0 - 0.005 \cdot Z$. The dots A, B, C and D correspond to the heights 0.84 m, 4.4 m, 24.4 m and 62.6 m respectively. The hodographs are shown after
1. t = 0 h, 2. t = 5 min, 3. 1 h, 4. 2 h, 5. 3 h, 6. 4 h and 7. 5 h.

Vindhodografer. Bakgrundsvinden är initialt $u^* = 5$ m/s, $v^* = 0$. Modellen initialiseras varefter bakgrundsvinden plötsligt ändras till $u^* = 0$, $v^* = 15$ m/s. Under denna körning är $Z_0 = 0.01$ m, $T^* = 283.0 - 0.005$ Z. Punkterna A, B, C och D visar respektive höjderna 0.84 m, 4.4 m, 24.4 m och 62.6 m. Vindhodograferna är tagna efter 1. t = 0 t, 2. t = 5 min, 3. 1 t, 4. 2 t, 5. 3 t, 6. 4 t och 7. 5 t.

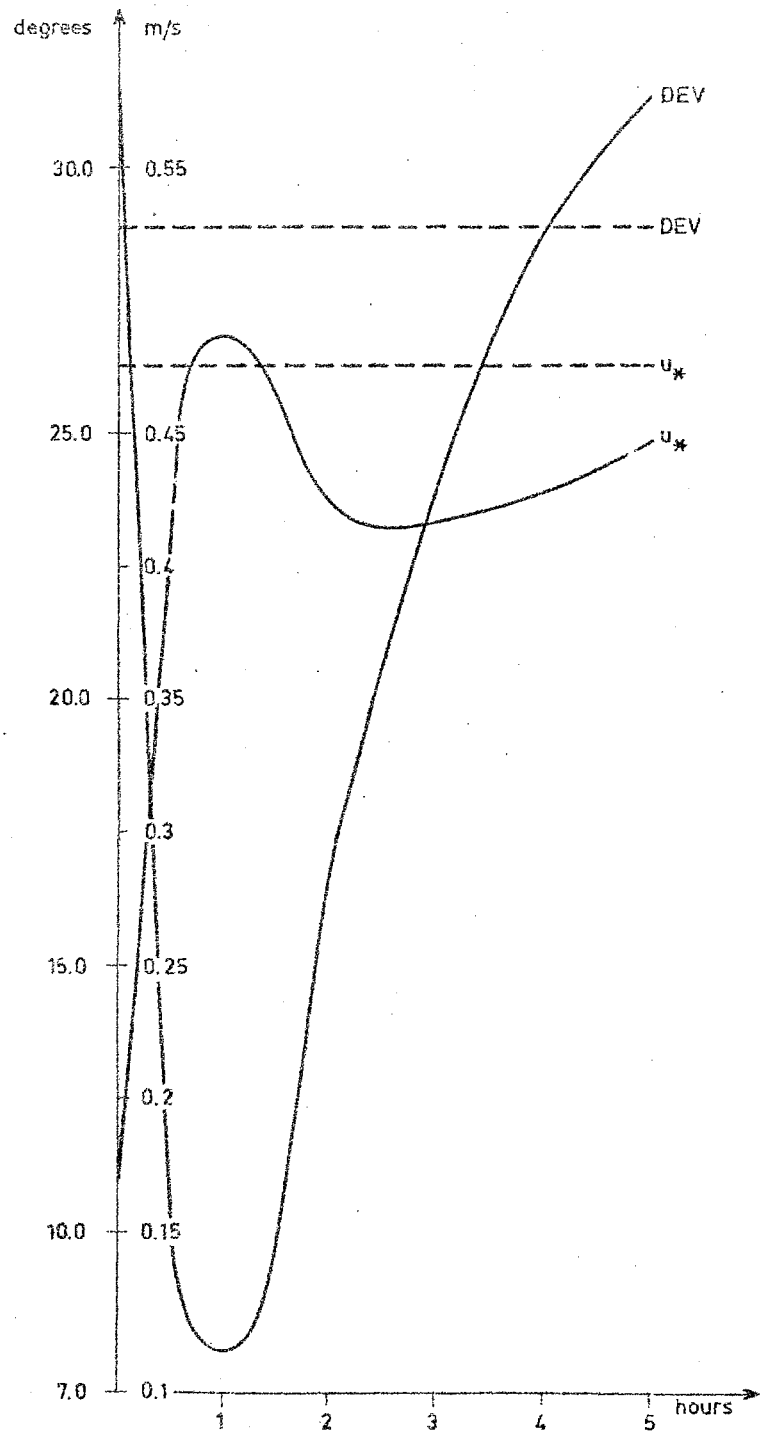

Fig. 8 Friction velocity and deviation angle for the sudden change in background wind experiment. Full curves show results from the unsteady computations and dashed curves from the corresponding steady state results.

Friktionshastigheten och tvärisobara vinkeln för experimentet med en plötslig ändring i bakgrundsvinden. De heldragna kurvorna visar resultaten från de icke-stationära beräkningarna medan de streckade visar de motsvarande stationära resultaten.

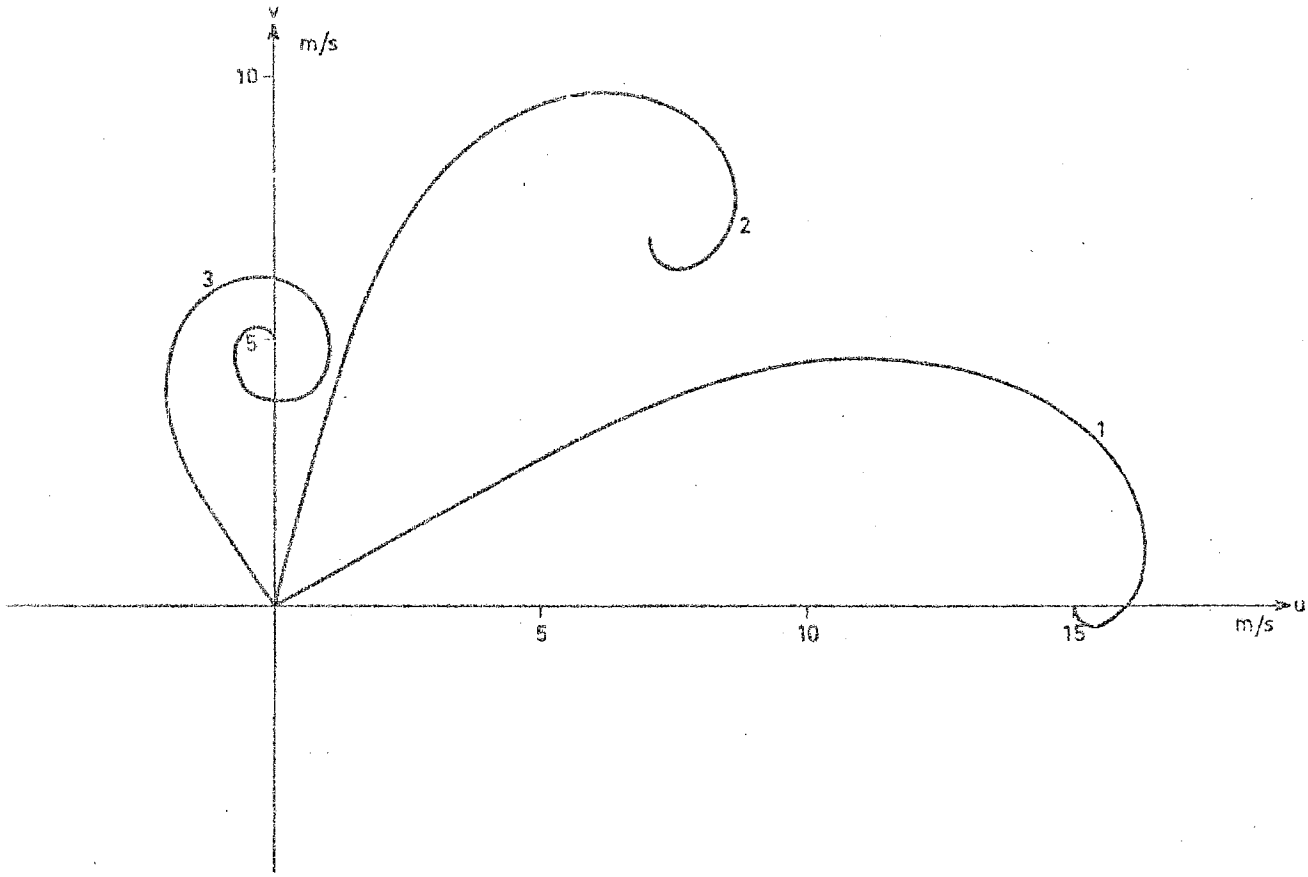

Fig. 9 Wind hodographs. The background wind is given by

$$u^* = |\mathbb{V}^*| \cos(\alpha t) \qquad \alpha \text{ correponds to a period of 24 h}$$

$$v^* = |\mathbb{V}^*| \cdot \sin(\alpha t)$$

$$|\mathbb{V}^*| = 10 \cdot \frac{t}{12}\ ,\ t \text{ in hours. } Z_0 = 0.01 \text{ m and } T^* = 283.0 - 0.005 \cdot Z.$$

The model is started from initialized wind and K profiles. The wind hodographs are shown after 1. t = 0, 2. t = 6 h and 3. 12 h.

Vindhodografer. Bakgrundsvinden är given av

$$u^* = |\mathbb{V}^*| \cos(\alpha t) \qquad \alpha \text{ motsvarar en period av 24 t}$$

$$v^* = |\mathbb{V}^*| \cdot \sin(\alpha t)$$

$$|\mathbb{V}^*| = 10 \cdot \frac{t}{12}\ ,\ t \text{ i timmar. } Z_0 = 0.01 \text{ m och } T^* = 283.0 - 0.005 \cdot Z.$$

Integrationen har startats från initialiserade vind- och K-profiler. Vindhodograferna är tagna efter 1. t = 0, 2. t= 6 t och 3. 12 t.

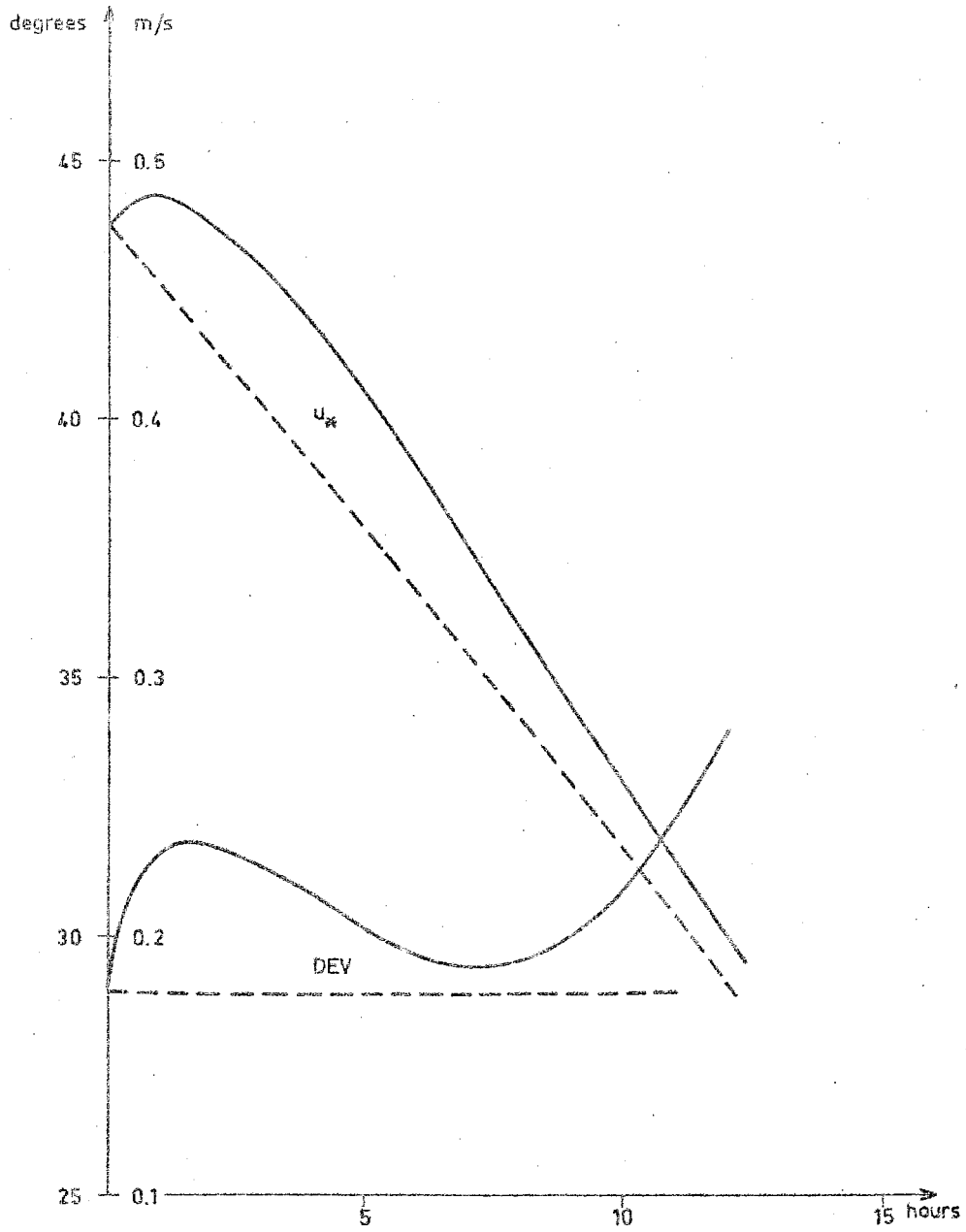

Fig. 10 Friction velocity and deviation angle as a function of time. Background wind as in fig. 9. Full curves show unsteady and dashed curves steady state results.

Friktionshastighet och tvärisobara vinkeln. Bakgrundsvinden densamma som i fig 9. Heldragna kurvor visar icke-stationära och streckade stationära resultat.

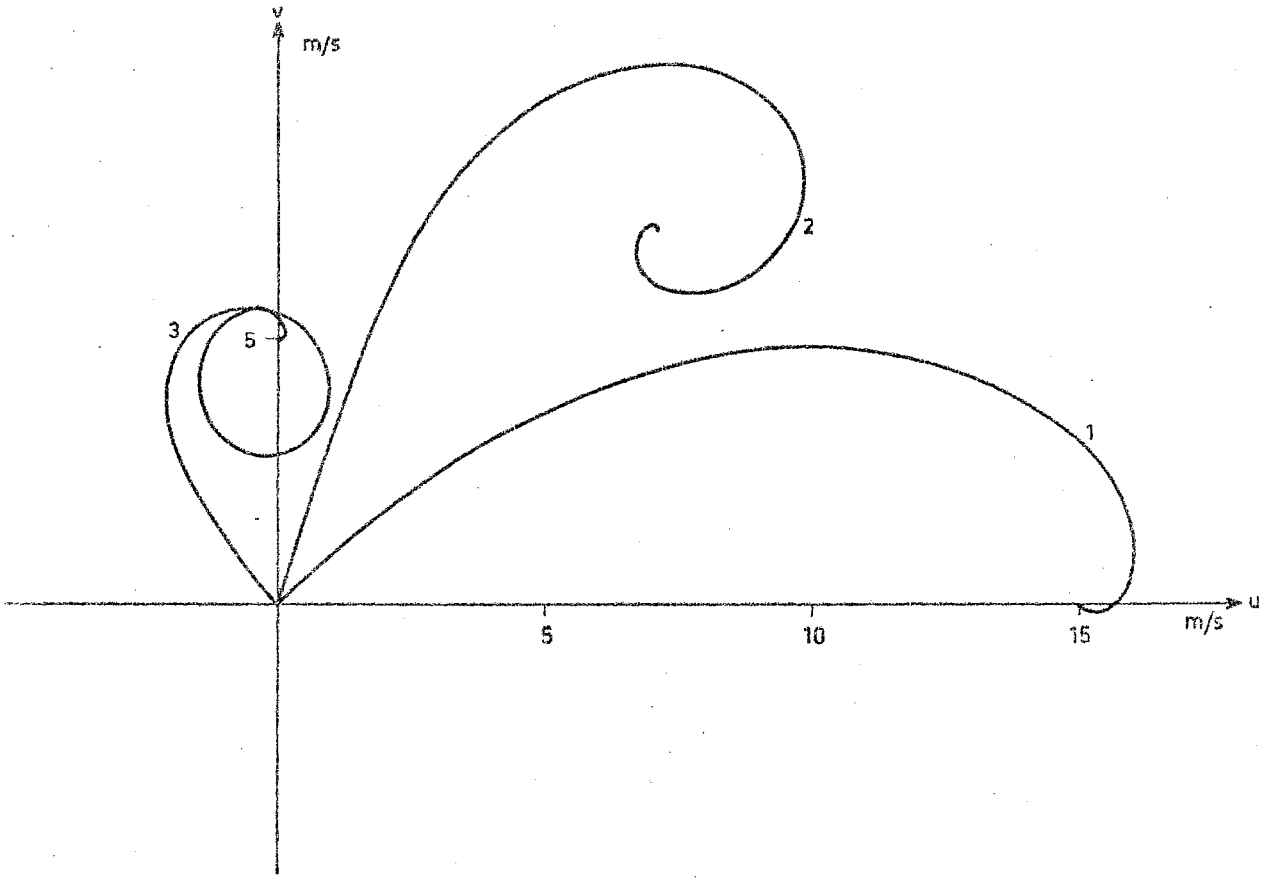

Fig. 11 The same as for fig. 9 but the integration is started from and Ekman-profile with K_m = constant.

Samma som i fig 9 men integrationen har startats från en Ekman-profil med K_m = konstant.

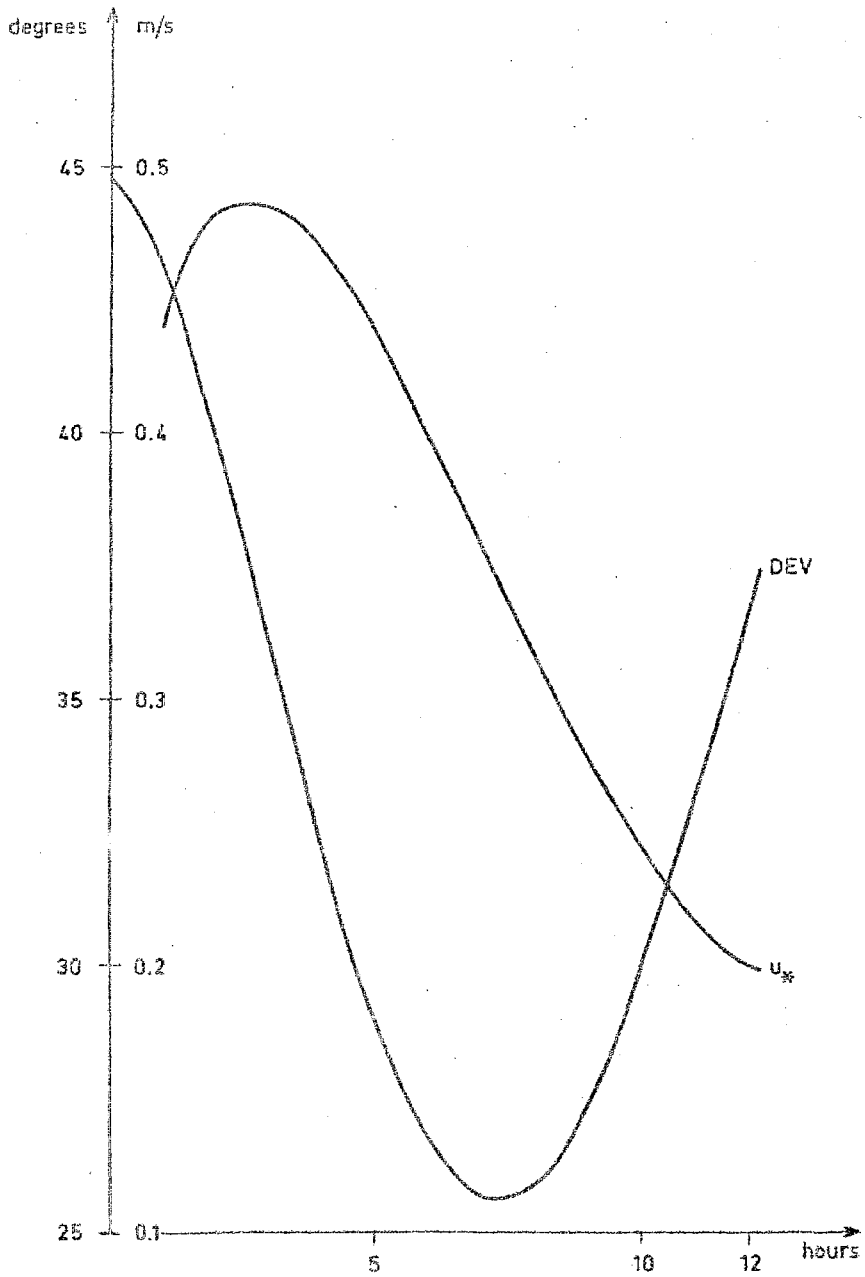

Fig. 12 The same as for fig. 10. Initial Ekman-profile.

Samma som för fig 10. Initial Ekman-profil.

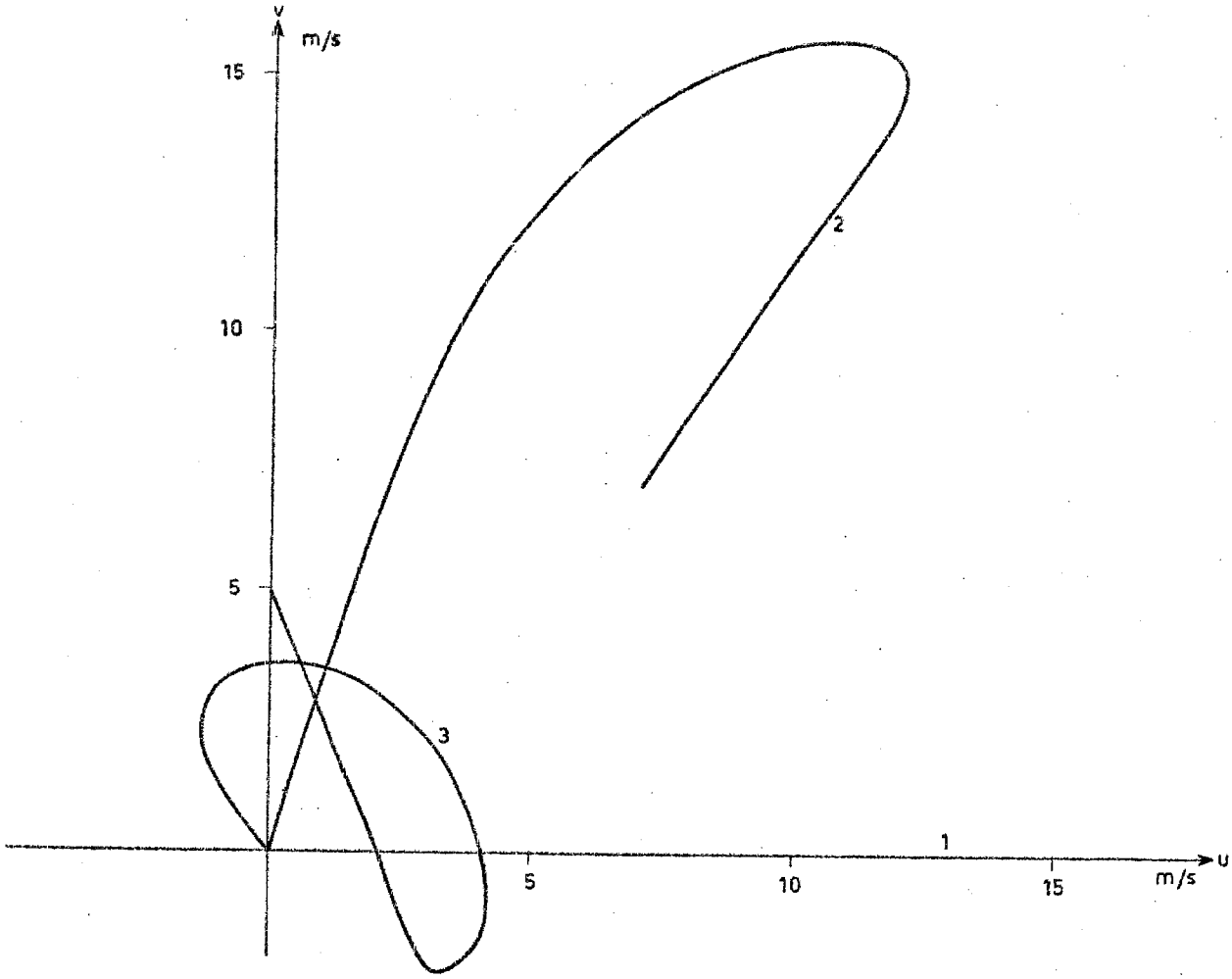

Fig. 13 The same as for fig. 11 and 9 but the initial wind is given by $u' = 15 \cdot \frac{Z}{H} - 15$, $v' = 0$.

Samma som för fig 11 och 9 men med initiala vinden given av $u' = 15 \cdot \frac{Z}{H} - 15$, $v' = 0$.

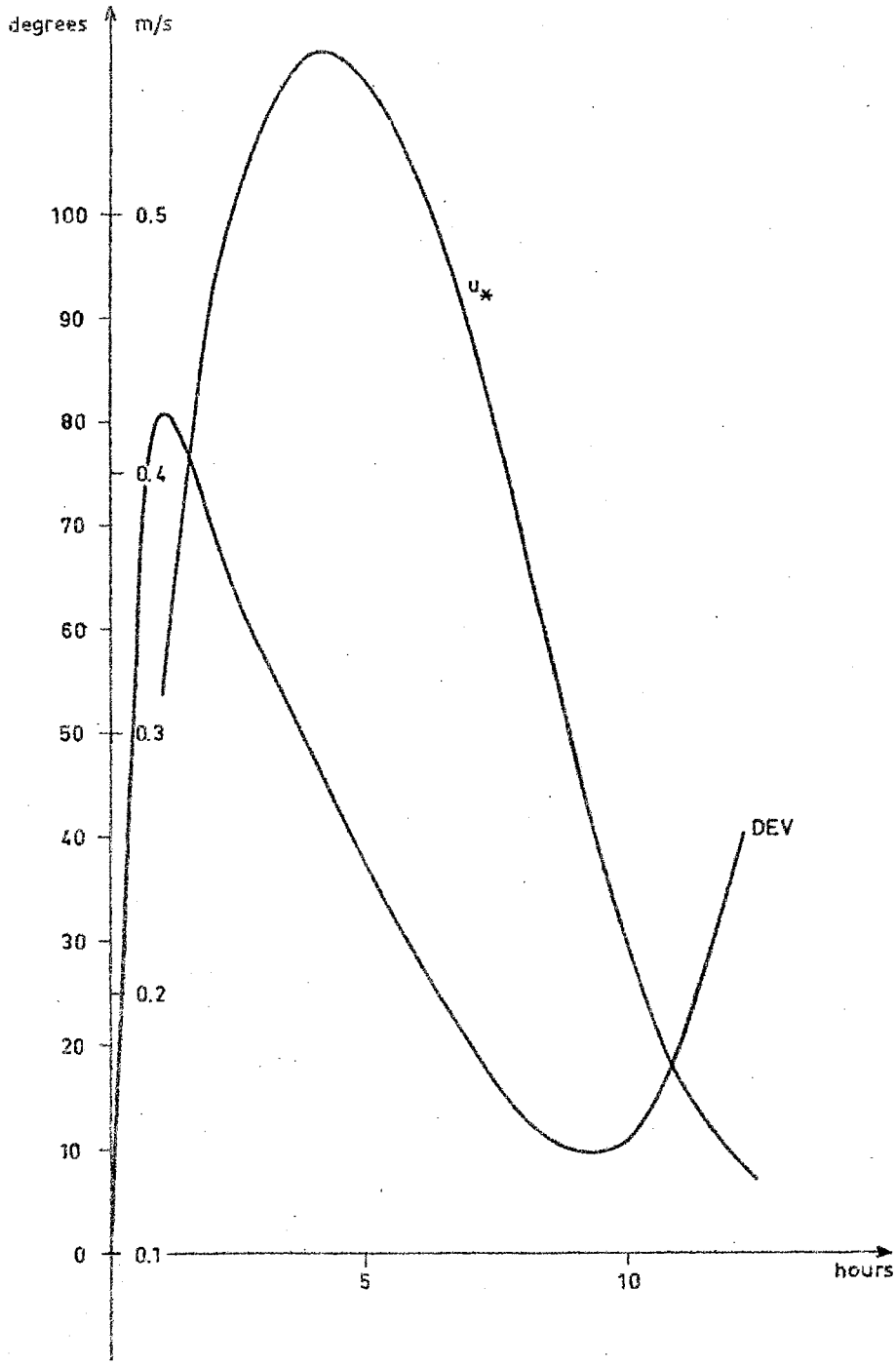

Fig. 14 The same as for fig. 10. Initial data as in fig. 13.

Samma som för fig 10. Initialdata som i fig 13.

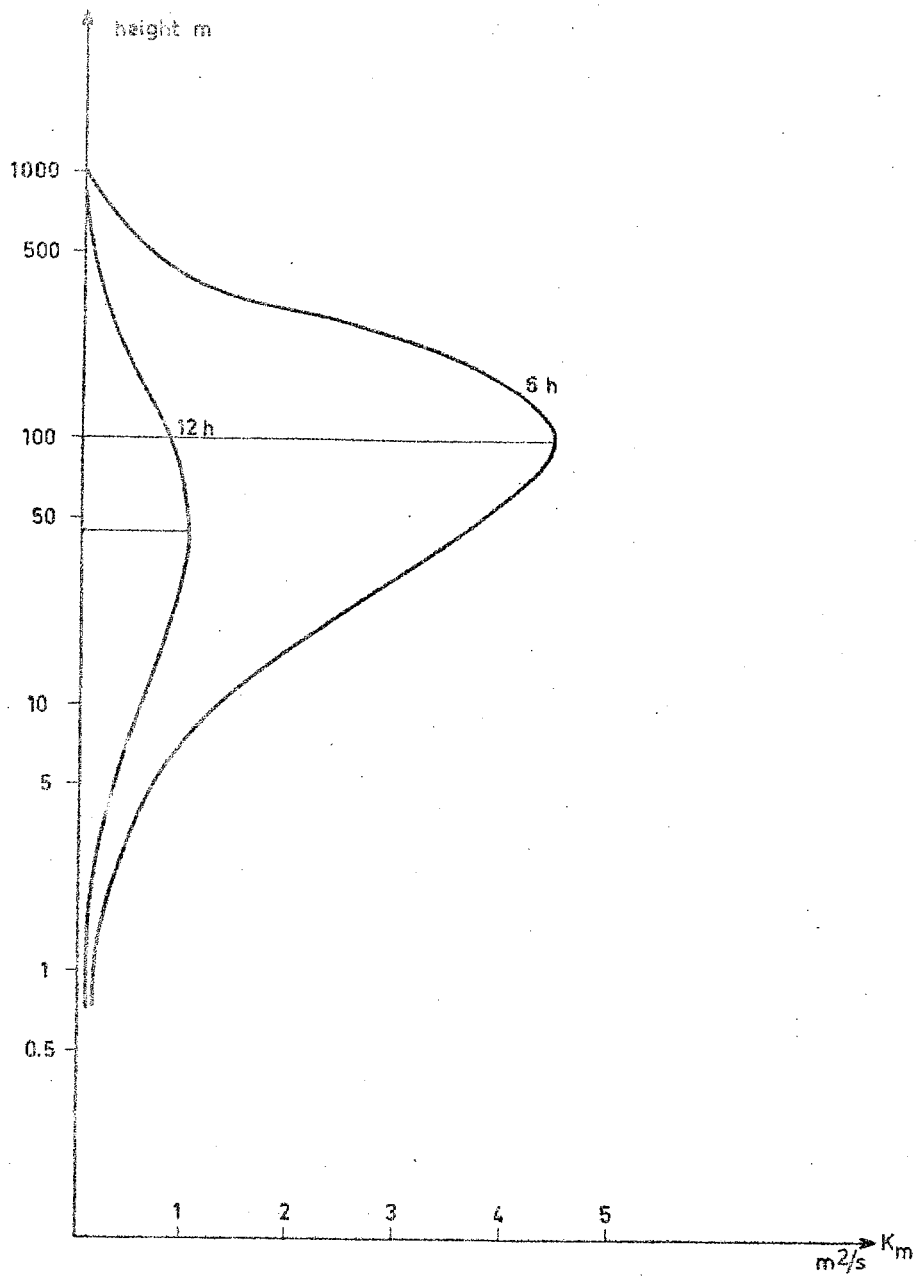

Fig. 15 Eddy exchange coefficient profiles after 6 and 12 hours. Initial Ekman-profile.

Profiler för turbulenta utbyteskoefficienten efter 6 och 12 timmar. Initial Ekman-profil.

References

Businger et al, 1971, Flux-Profile Relationships in the Atmospheric surface layer., Journal of the Atmospheric Sciences, March 1971, Vol 28

Blackadar, A K, 1962, The vertical distribution of wind and turbulent exchange in a neutral atmosphere., Journal of Geophysical Research, Vol 67, No 8

Carslaw, H S, 1921, The Mathematical theory of the conduction of heat in solids, Mc Millan and Company

Ching, J K S & Businger, J A, 1968, The response of the planetary boundary layer to time varying pressure gradient force, Journal of the Atmospheric Sciences, November 1968, Vol 25

Clarke, R H et al, 1971, The Wangara experiment: Boundary Layer Data., Div of Met Phys Tech Paper No 19, CSIRO, Australia

Deardorff, J W, 1972, Numerical investigation of neutral and unstable planetary boundary layers., Journal of the Atmospheric Sciences, January 1972, Vol 29

_____, 1973, The use of subgrid transport equations in a three dimensional model of atmospheric turbulence., Journal of Fluid Engineering, Februari 1973

Delage, Y, 1973, A numerical study of the nocturnal atmospheric boundary layer, Paper presented at the symposium on the Atmospheric Boundary Layer in Mainz, Germany Oct 10-12, 1973

Estoque, M A, 1963, A numerical model of the atmospheric boundary layer., Journal of Geophysical Research, No 4, Vol 68

Gutman, L N, 1969, Introduction to the non-linear theory of meso scale meteorological processes., Leningrad, 1969 (english translation: Israel Program for Scientific Translations, Jerusalem 1972)

Karlsson, E, 1972, A numerical model for the boundary layer of the atmospheric at neutral and stable stratification., DM-report No 7, Institute of Meteorology, University of Stockholm (in Swedish)

Lykosov, V N, 1972, Unsteady state in the planetary boundary layer of the atmosphere., Izv, Atmospheric and Oceanic physics, Vol 8, No 2

Melgarejo, J W & Deardorff, J W, 1974, Stability Functions for the Boundary-Layer Resistance Laws based upon observed Boundary-layer heights., Journal of the Atmospheric Sciences, Vol. 31, No 5, July 1974.

Pandolfo et al, 1965, The development of a numerical prediction model for the planetary boundary layer., Travellers Research Center, Inc.Report 7465-174

Peagle, J & Rasch, G E, 1973, Three-dimensional characteristics of diurnally varying boundary-layer flows., Monthly Weather Review, Vol 101, No 10

Richtmayer, R D & Morton, K W, 1967, Difference methods for initial-value problems., John Wiley & Sons

Sasamori, T, 1970, A numerical study of atmospheric and soil boundary layers., Journal of the Atmospheric Sciences, Vol 27, Nov 1970

Shaffer, W A & Long, P E, 1973, A predictive boundary layer model. Paper presented at the Symposium on the Atmospheric Boundary Layer in Mainz, Germany Oct 1973

Taylor, P A, 1969, The planetary boundary layer above a change in surface roughness., Journal of the Atmospheric Sciences, Vol 26, May 1969

Young, J A, 1973, A theory for isallobaric air flow in the planetary boundary layer., Journal of the Atmospheric Sciences, Vol 30, No 8

Zdunkowski, W G & Barr, A E, 1972, A radiative-conductive model for the prediction of radiation fog., Boundary-layer Meteorology, No 3, 1972

Zilitinkevich, S S & Deardorff, J W, 1974, Similarity theory for the planetary boundary layer of time dependent height. Journal of the Atmospheric Sciences, Vol. 31, No 5, July 1974.

NOTISER OCH PRELIMINÄRA RAPPORTER. Serie METEOROLOGI

Nr 1 K a r l s s o n, K E, Instrumentella och visuella åskobservationer. (1960)

Nr 2 T h o m p s o n, T, Den naturliga radioaktivitetens variation med vädret. (1961)

Nr 3 M o d é n, H, Jämförelse mellan olika instrumentuppställning vid Gamla Observatoriet i Stockholm. (1963)

Nr 4 P e r s h a g e n. H, Snöförhållandenas svårighetsgrad under vintrarna 1931-1960. (1963)

Nr 5 M o d é n, H, Stockholms temperaturserie. (1963)

Nr 6 B e r g g r e n, R, En statistisk undersökning av vindriktningens vertikala variation i övre troposfären. (1963)

Nr 7 W a l l é n, C C, Sannolikheten för olika mängder av dygnsnederbörd i Sverige. (1963)

Nr 8 L i n d h o l m, F, Report on comparisons at Stockholm and Visby between the K Ångström original absolute scale and the new Smithsonian absolute scale for primary standard pyrheliometers. (1963)

Nr 9 M o d é n, H, Åskans dagliga period i Sverige. (1963)

Nr 10 Å n g s t r ö m, A, Some fundamental principles concerning calibration and standardization of pyrheliometers. (1964)

Nr 11 R o d h e, B, Comparison of pyrheliometers at different turbidity conditions. (1964)

Nr 12 S j ö l a n d e r, G, En statistisk undersökning av kuling och storm i svenska farvatten. Del 1, Västkusten norra delen. (1965)

Nr 13 T h o r s l u n d, B, Isförhållanden i svenska farvatten under normalperioden 1931-1960. (1966)

Nr 14 E r i k s s o n, B, Sannolikhetsfördelningar av temperatur, nederbörd och vind vid olika väderlekstyper. (1967)

Nr 15 T h o r s l u n d, B, Havsisens utbredning i Bottniska viken, Östersjön, Kattegatt och Skagerack under isvintrarna 1951/52-1966/67. (1967)

Nr 16 S c h m a c k e, E, Blixträkning med instrument. Synpunkter jämte preliminära resultat av timregistrering av blixtaktiviteten i södra Sverige under åren 1962-1966. (1968)

Nr 17 P o h l m a n, J, En statistisk undersökning av kuling och storm i svenska farvatten. Del 4, Farvattnen kring Gotland och norra Öland. (1968)

Nr 18 L u n d q v i s t, J-E, Isförhållanden i Vänern under perioden 1940-1963. (1969)

Nr 19 R o d h e, B, Comparison of the standard pyrheliometer Å 158 with the sub-standard instrument Å 70 and Å 171. (1969)

Nr 20 R o d h e, B, Simplified formulae for computation of the turbidity coefficient. (1969)

Nr 21 S a l o m o n s s o n, G, En statistisk undersökning av kuling och storm i svenska farvatten. Del 3, södra Östersjön. (1969)

Nr 22 H o l m s t r ö m, I, Extrapolation of meteorological data. (1969)

Nr 23 J o e l s s o n, R, Applicering av empiriska ortogonala funktioner på en synoptisk vädersituation. (1970)

Nr 24 L ö n n q v i s t, O, MASKINELL PROGNOSTEXT: Ett experiment med i datamaskin formulerade väderrapporter. (1971)

Nr 25 N y b e r g, A och H å r s m a r, P-O, Mätningar av avdunstning- kondensation samt snösmältning från en snöyta. (1971)

Nr 26 P e r s s o n, Anders O, En enkel metod att beräkna rådande vertikalvind och nederbördsintensitet ur aerologiska vind- och fuktighetsdata. (1971)

Nr 27 H e n r i k s o n, A-B, An investigation of the accuracy in numerical computations of horizontal trajectories in the atmosphere. (1971)

Nr 28 A x e l s s o n, G, Studium av infraröda (IR) satellitfotografier mottagna vid SMHI vintern 1971 samt en resumé av indirekt bestämning av atmosfärens vertikala temperaturprofil med hjälp av strålningsdata från satelliter. (1971)

Nr 29 S c h m a c k e, E, FRÅN METEOROLOGINS GRYNING. Några drag i forntidens meteorologi. (1971)

Nr 30 L ö n n q v i s t, O, Några glimtar från Svensk klimatologi under 1700- och 1800-talet. (1972)

Nr 31 B l e c k e r t, G och M o e n, L, Meteorologisk ADB-verksamhet vid SMHI. (1972)

Nr 32 E r i k s s o n, B, Temperatur- och nederbördsförhållanden i Sverige 1961-70 i relation till perioden 1931-60. (1972)

Nr 33 B o d i n, S, A quasi-geostrophic 3-parameter numerical prediction model in empirical orthogonal functions. (1972)

Nr 34 R o d h e, B, The procedure of reading the Ångström Compensation Pyrheliometer. (1972)

Nr 35 J a k o b s o n, L, Verifikation av prognoser av dygnsmedeltemperaturen för Stockholmsområdet. (1973)

SMHI Rapporter, METEOROLOGI OCH KLIMATOLOGI (RMK)

Nr 1 T h o m p s o n, T, U d i n, I, och O m s t e d t, A, Sea surface temperatures in waters surrounding Sweden. (1974)

Nr 2 B o d i n, S, Development of an unsteady atmospheric boundary layer model. (1974)